1992

Analytical and numerical modeling of a graded band gap amorphous silicon based p-i-n solar cell

Greg Fick Baldwin
Iowa State University

Analytical and numerical modeling of a graded band gap amorphous silicon based p-i-n solar cell

by

Greg Fick Baldwin

A Thesis Submitted to the
Graduate Faculty in Partial Fulfillment of the
Requirements for the Degree of
MASTER OF SCIENCE

Department: Electrical and Computer Engineering
Major: Electrical Engineering

Iowa State University
Ames, Iowa

1992

TABLE OF CONTENTS

I. INTRODUCTION

A. Purpose of Research

High efficiency amorphous solar cells are a valuable technology researched world wide. Cell efficiency has been reported as high as twelve and thirteen percent initially, then stabilizing at about nine percent over extended exposure to sunlight.[1] If the efficiency can be raised to a stable fifteen percent, the low cost of these cells will allow them to compete with fossil fuels in the consumer energy market. Large scale production of hydrogenated amorphous silicon modules has already been reported. Much of the current research is directed toward improving the efficiency and stability. The work presented here introduces a new method for guiding the design of high efficiency hydrogenated amorphous solar cells, and may be used in conjunction with new fabrication methods that produce material with greater stability.

B. Background on Computer Modeling

The most important parameter in determining cell efficiency in hydrogenated amorphous silicon (a-Si:H) alloy p-i-n solar cells is the electric field profile, which is highly non-uniform. The value of the field at each point determines how far the photogenerated carriers can travel before recombining, and is determined by the trapped charge density. The method for accurately predicting the charge density and field profile is outlined in Chapters 2 and 3, and requires a numerical solution to Poisson's equation.

Initial studies on a-Si:H p-i-n devices estimated the electric field by various methods. Dalal and Alvarez used a uniform field approximation for the

i-layer electric field by dividing the sum of the applied and diffusion voltages by the thickness of the i-layer.[2] This approximation, also used later by Crandall, is easy to use since computer models are not required, but can lead to large errors in some cases.[3] For example, if the i-layer has a high charge density due to exposure to sunlight, the electric field may drop to zero for much of the region, causing a large reduction in collection efficiency.

An improved method was proposed recently by Dalal et al., which estimates the electric field by solving Poisson's equation for a charge density that changes exponentially with distance into the i-layer.[4] This method does produce more accurate estimates for the electric field profile, but the actual charge density does not follow a simple exponential distribution since the density of states changes exponentially with energy in the middle of the band gap. This method is easy to use, since no numerical integrations are required, but since the electric field profile is very important in determining the efficiency, more accurate models are better suited for the design process.

To solve the electric field profile for an energy dependent density of states, Hack and Shur built a successful computer model in 1984.[5] Their model also included the effects of non-uniform doping profiles and non-uniform optical excitation. After finding a complete self-consistent solution to the transport equations for the entire p-i-n structure using numerical methods, they could accurately predict the short circuit current, open circuit voltage, and fill factor for a constant band gap material. Their model also includes the p-i and i-n boundary conditions, the effects of various recombination mechanisms, and the effects of the presence of charge carriers on the electric field profile. These parameters are not well known in graded band gap material, though, so this

model is used primarily for characterizing constant band gap solar cells.

The goal of this report is to accurately reproduce the electric field profile for an energy-dependent density of states, then to use this profile to predict the collection efficiency by solving a field-dependent diffusion equation for many different device structures including graded band gap devices. This method reduces the number of parameters affecting cell efficiency so that the effects of various new structures and conditions can be studied. Neglecting the boundary conditions results in somewhat lower values for the electric field near the interfaces, but this will have only a minor effect on the efficiency since the field is normally sufficiently high to collect all of the charge carriers in this region. In chapter 4, a comparison of the electric fields produced by the method described in Chapter 3 and by Hack and Shur's model shows that the fields are sufficiently close, and the resulting quantum efficiency curves will be reasonably accurate. This is also verified by reproducing the results of experimental reports on the efficiency of various device structures.

It should be noted that the fields of Hack and Shur are held nearly constant at the p-i and i-n interfaces for increasing bias voltage due to the boundary conditions and are lowered in the middle of the region by the presence of charge carriers. The simplified model presented here does not consider these conditions, but still produces similar electric field profiles. The advantage of using a simplified model to find the electric field is that now the effects of various changes such as band gap profile and defect density can be easily studied.

Once the model is shown to reproduce experimental results, various new device structures are tested and evaluated. A method for optimizing the

efficiency for a given set of parameters unique to a particular growth system is outlined, and a specific example is given, showing the usefulness of this simplified approach.

II. PHYSICS OF AMORPHOUS SILICON MATERIALS AND DEVICES

A. Effects of Positional Disorder

A complete review of amorphous semiconductor materials can be found in Madan and Shaw, and a brief overview is presented here.[6] Amorphous semiconductor material is characterized by the large amount of positional disorder among its constituent atoms. Short range order is retained, since atoms will have approximately the same number of nearest neighbors throughout the material. Thus, for silicon, an atom still has four surrounding atoms. Each of those atoms has three additional atoms around it, but the same is not true for those additional atoms. Broken and distorted bonds cause the loss of long range order by the third shell.[6]

The energy-wave vector (E-k) diagram retains its validity for such a system, but no longer has a periodic structure.[7] Thus, systems with an indirect band gap in the crystalline state, now only have a direct band gap in the amorphous state. The conduction and valence bands creating this band gap contain extended states allowing free electron and hole travel. Between the bands are a large number of localized states that can act as traps and recombination centers.

Positional disorder causes the direct band gap to be narrower in amorphous material than in crystalline material. The electron wave functions around the constituent atoms are different from atom to atom due to the varying energies associated with distorted and broken bonds. When these unequal adjacent wave functions interact, they split farther apart in energy than equal wave functions would. As a result, the valence band moves up in energy and

the conduction band moves down in energy. For the amorphous silicon system (a-Si), the band gap is around 1.7 eV to 1.8 eV, while the direct band gap for crystalline silicon is around 3.0 eV.

Because there is a continuous density of states from the valence band to the conduction band, there essentially is no forbidden gap in energy levels in amorphous material, as shown in Figure 1. The distinction between the conduction band and the valence band can be made in two ways. First, the mobility of charge carriers drops when the states change from extended states to localized states. This occurs because the carrier movement changes from free transfer between extended band states, to 'hopping' between the localized states. The energy between the bottom of the conduction band extended states and the top of the valence band extended states is known as the mobility gap.

Second, an optical gap can be defined by the dependence of the absorption coefficient . The point in each band where the DOS begins to fall exponentially marks the extent of that band. For light with energies greater than the optical gap, the absorption coefficient increases directly with increasing light

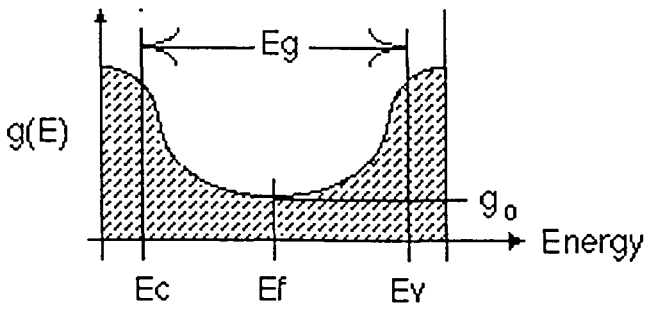

Figure 1. Schematic representation of the energy-dependent midgap density of states

energy. For light with energies less than the optical gap, the absorption coefficient falls exponentially with decreasing light energy. The band gap values used here will be the energy of the mobility gap, which are usually somewhat smaller than the optical gap.

B. Sources of Midgap States

Density of States

The energy dependent DOS between the conduction and valence bands has two exponentially increasing regions as shown in Figure 2. Region A of Figure 2 shows the beginning of the localized states above the valence band. These states have a large decreasing energy slope, and are known as the valence band tail. The corresponding conduction band tail is shown in region D. Regions B and C are deep level states with a smaller energy slope. They generally meet near the middle of the mobility gap at an energy density of g_o. The energy level where g_o is located is also the fermi level in intrinsic material, unless defect states at other levels appear. The defect levels created

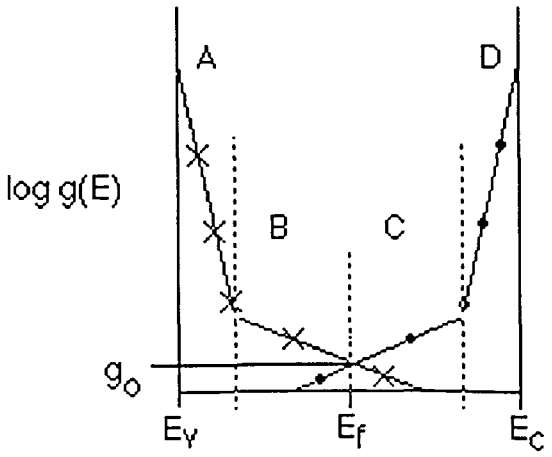

Figure 2. Logarithmic DOS diagram of band tails and deep level states

by doping will cause the fermi level to move toward the valence or conduction band, which results in band bending at dopant junctions such as the p-i and i-n interfaces of solar cell with the p-i-n doping structure.

The deep level energy-dependent DOS of regions B and C can be represented by:

$$g(E)=g_o\exp(\frac{E}{E_a}) \qquad (1)$$

where E_a is the characteristic energy slope of the exponential distribution. The values of g_o and E_a depend on the conditions of growth and can be determined experimentally.

The actual midgap DOS is generally more complicated than shown in Figure 2, with large defect densities at specific energy levels. Pure a-Si has a very large DOS near the center of the gap. These states act as recombination centers, rendering the material useless for devices. The states are created by silicon atoms with only three nearest neighbors. The fourth unpaired electron in the silicon valence shell, known as a dangling bond, becomes the recombination center.

In 1972, Spear and LeComber grew hydrogenated a-Si (a-Si:H) by the glow discharge decomposition of SiH_4.[8] The excess hydrogen present during growth bonded covalently with the silicon dangling bonds, effectively lowering the midgap DOS. Now, a-Si:H and its alloys are the primary materials used for amorphous devices. The presence of hydrogen in the material also changes the band gap according to the relationship shown in Figure 3.[9] The highest quality a-Si:H has a hydrogen content of eight to ten percent, since less

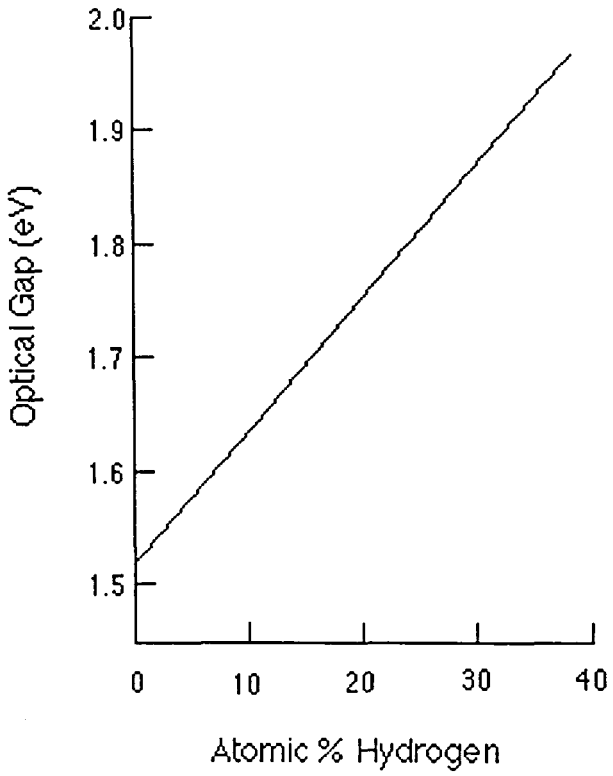

Figure 3. Relationship between hydrogen content and the optical energy gap

hydrogen leaves too many dangling bonds, while greater hydrogen content creates new midgap defect states. Equation 1 is a good representation of the midgap DOS in high quality a-Si:H, with a g_o value around 10^{15} $cm^{-3}eV^{-1}$.

Amorphous material can be doped both p-type and n-type, usually with boron and phosphorous respectively. Heavily doped material for ohmic contacts can be achieved by high power gas phase decomposition, which produces micro-crystalline material. This material has high values of conductivity suitable for the p^+- and n^+-layers of a p-i-n solar cell.

The presence of dopant atoms creates additional disorder in amorphous material, which produces new defect levels as shown in Figure 4.[6] These defect levels can quickly reduce built-in junction fields, and cause carrier

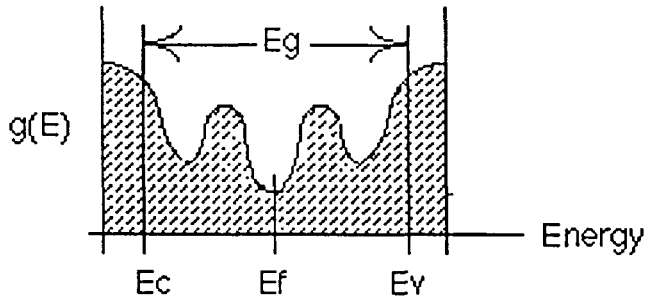

Figure 4. Midgap DOS diagram with defect levels

recombination, so the middle of the i-layer must be kept as free of dopant atoms as possible. High defect levels are tolerable in the p^+- and n^+-layers, since they have only one type of carrier and are short in length.

The band gap of a-Si:H can be changed by alloying with other elements. The most commonly used elements for changing the band gap in a-Si:H are germanium and carbon. Narrow band gap material is made with a-(Si,Ge):H, and can reach an energy as low as 1.1 eV. Wide band gap material is made with a-(Si,C):H, and can be as high as 2.5 eV. The presence of Ge and C creates new defects in the material, though, resulting in higher values of g_o. Thus, the transport parameters (mobility, lifetime) for alloyed material will be lower due to the additional recombination centers. This transport degradation limits the amount of Ge and C that can be added to the i-layer material with the practical limits for the band gap at about 1.5 eV minimum to 1.8 eV maximum.

One other source of midgap states, exposure to sunlight, results in the degradation of efficiency over time, as previously mentioned. Staebler and Wronski first characterized this effect by exposing amorphous material to sunlight and measuring the fall in efficiency.[10] To explain this effect, Adler

proposed the idea that the incoming photons provided energy to repopulate existing defect states in the amorphous structure with charge.[11] Supported by recent data, this idea indicates that a large charge density will be present in amorphous material immediately after exposure to sunlight.[12]

Another model shows that extended exposure to sunlight can also break weak hydrogen-silicon bonds creating dangling bond defects. These defects capture charge carriers and further decrease the electric field in the i-layer.

These charges also reduce the transport parameters in addition to lowering the electric field in the i-layer, effectively decreasing the efficiency over time. Preventing this process from happening by removing the defect states during growth may be a way to increase stability, and a method for doing this is outlined in appendix A.

C. Light Absorption.

The large absorption coefficients of a-Si:H and its alloys are one of the reasons they are suitable for solar cell devices. Figure 5 demonstrates how the absorption coefficient (α) depends on the photon energy for a given optical band gap. The value of α for the band to band transitions of region A in Figure 5 can be modeled by:

$$\alpha h\nu = B^2(h\nu - E_g)^2 \qquad (2)$$

where $h\nu$ is the photon energy, E_g is the optical gap energy, and the prefactor B is defined by:

$$B^2 = \frac{4\pi\sigma_{min}}{ncE_w} \qquad (3)$$

where σ_{min} is the minimum metallic conductivity, n is the index of refraction, and E_w is the extent of the band tailing.[6] The magnitude of the prefactor B is about 750 $cm^{-1/2}eV^{-1/2}$. This relation holds for photons with energy equal to and greater the optical gap or about 0.1 eV larger than the mobility band gap.

The exponentially decreasing absorption coefficients from electron transitions near the edge of the mobility gap is shown in region B of Figure 5. This effect is commonly seen in all types of semiconductor materials, and is due to the exponential decrease in the DOS near the edge of the valence and

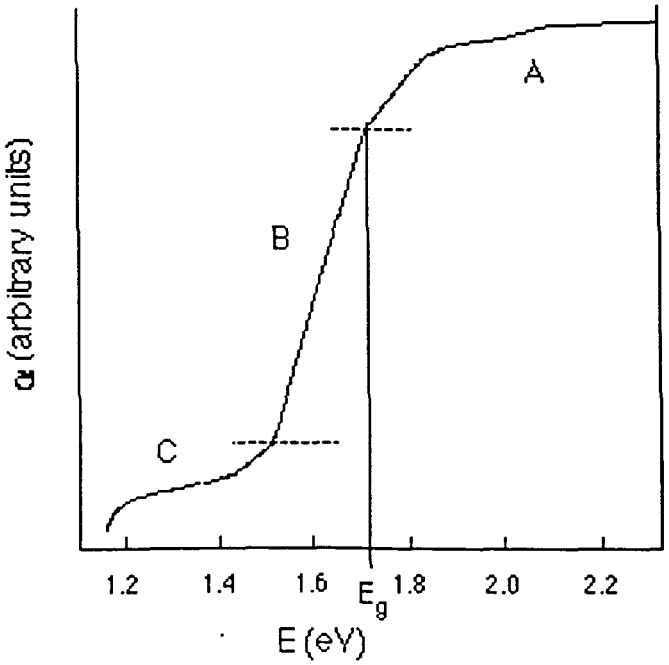

Figure 5. Relationship between the log of the optical absorption coefficient and photon energy

conduction bands. The absorption coefficient for this region follows the relationship:

$$\alpha = \alpha_o \exp(\frac{E}{E_o}) \qquad (4)$$

where E_o and α_o are determined experimentally. E_o is known as the Urbach energy and is generally around 0.045 eV for valence band tails and 0.025 eV for conduction band tails.

The absorption coefficients in region C of Figure 5 are produced by sub-band gap absorption, and are much smaller in magnitude. This region is not modeled since only wavelengths of 0.8 μm or less make significant contributions to the quantum efficiency in a-(Si,Ge):H devices.

D. Solar Cell Doping Structure

The standard p-n junction used for crystalline solar cells is shown in Figure 6. The wide base region is where most of the light is absorbed. Photogenerated holes must diffuse to the junction, where they are swept across by the built-in electric fields and collected. This structure does not work well for amorphous devices since most of the electron-hole pairs (ehps) in the base will recombine before they are collected. The high level of defect states in the doped material along with low transport parameters makes this recombination highly probable.

The addition of an intrinsic or undoped region between the p- and n-layers, shown in Figure 7, is required for high efficiency amorphous material. The i-layer effectively extends the built-in field created by the p- and n- layers,

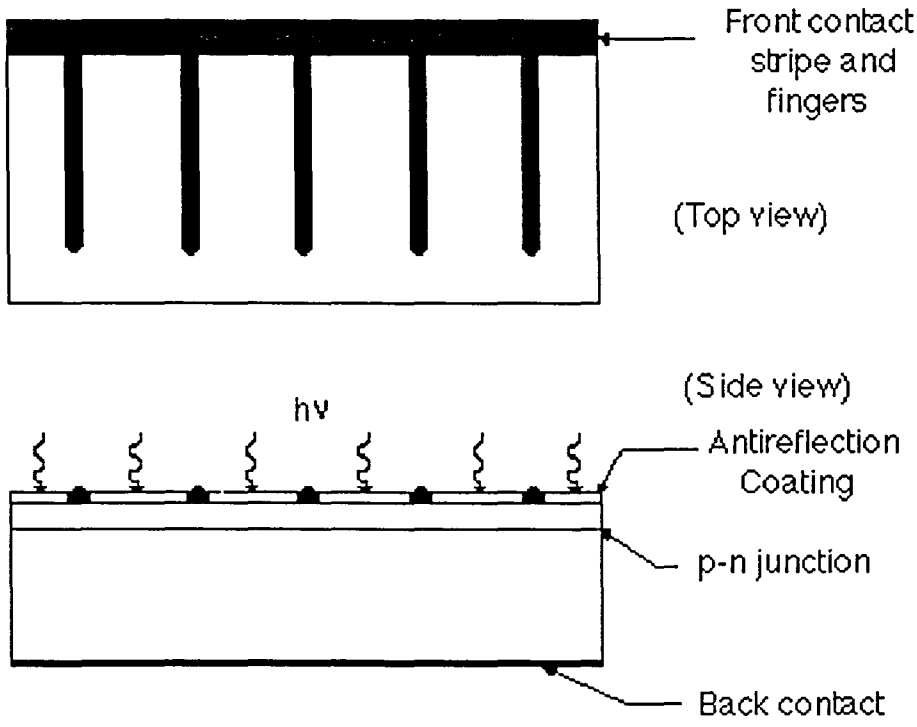

Figure 6. Schematic representation of a p-n junction solar cell

provided the i-layer has a low DOS. Light absorption now occurs primarily in this region since the p- and n-layers are thin (0.1μm). Photogenerated electron-hole pairs (ehps) are immediately subjected to the electric field, separated, and collected. Carrier collection has now become a high efficiency drift process, provided the field is sufficiently large throughout the i-layer.

E. Band Gap Grading

A constant band gap throughout the i-layer results in a typical band diagram shown in Figure 7. To operate the cell at maximum power, it is forward biased to a point near the open circuit voltage V_{oc}, as shown in Figure 8. To boost the output power closer to the ideal power point; in other words, increase

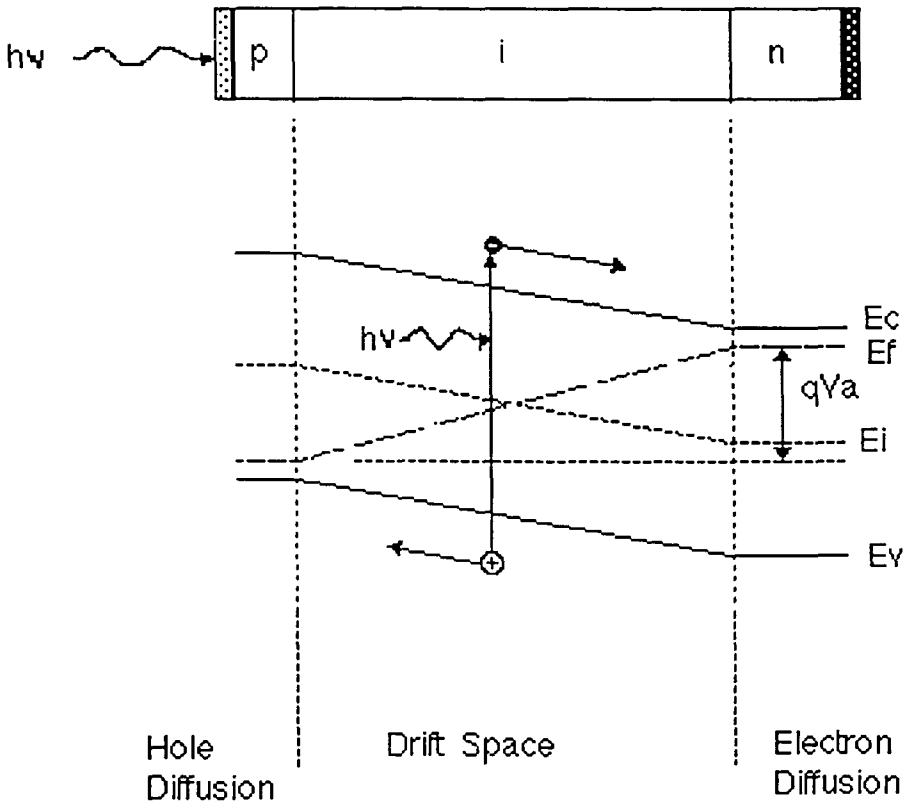

Figure 7. Schematic representation of a p-i-n solar cell and band diagram

the fill factor, the value of V_{oc} should be kept as high as possible. The ideal power point is simply the product of the short-circuit current I_{sc}, and V_{oc}. Then the fill factor is the maximum power ($I_m x V_a$ shown in Figure 8), divided by the ideal power.

To increase V_{oc}, the built-in voltage (V_{BI} shown in Figure 9) must be increased. Increasing the i-layer band gap at the p-i interface increases V_{BI}, and increases the efficiency. Wide band gap material has a lower absorption coefficient, though, according to equation 2. Therefore, the band gap can be graded to lower values for the rest of the i-layer. Band gap grading at the p-i

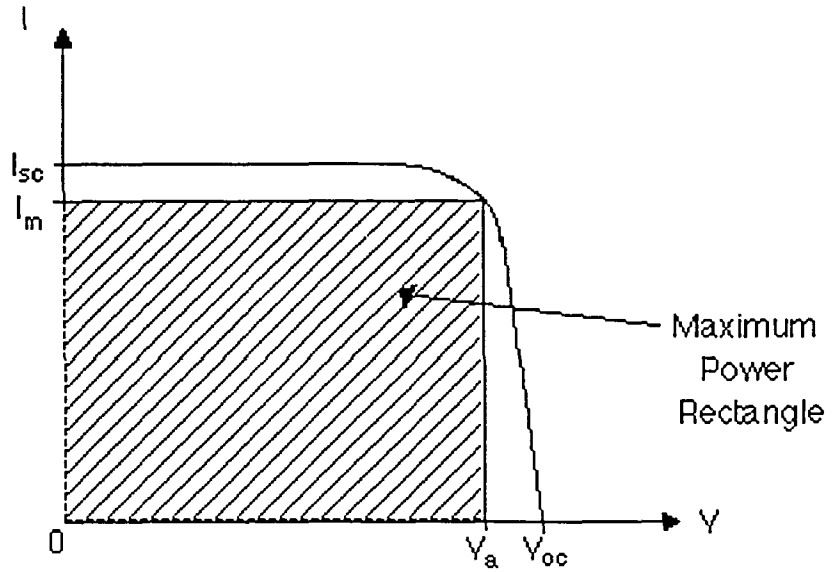

Figure 8. Inverted current-voltage relationship of an illuminated solar cell

interface also helps separate the photogenerated ehps. The electric field is generally high ($>10^5$ V/cm), in this region, but the large electron back diffusion toward the p-layer will promote recombination. The sloping band gap effectively increases the electric field by:

$$\varepsilon_{h,e} = \frac{\partial \Psi_{h,e}}{\partial x} \qquad (5)$$

where the left hand side is the slope of the valence band for 'hole diffusion' fields ε_h, and of the conduction band for 'electron diffusion' fields ε_e.

It is not clear from experimental data how the changing band gap is split between the valence band and the conduction band. For the fields used in this model, the split will be assumed to be equal between both bands.

As explained previously, a-Si:H alloys increase the midgap DOS, so the

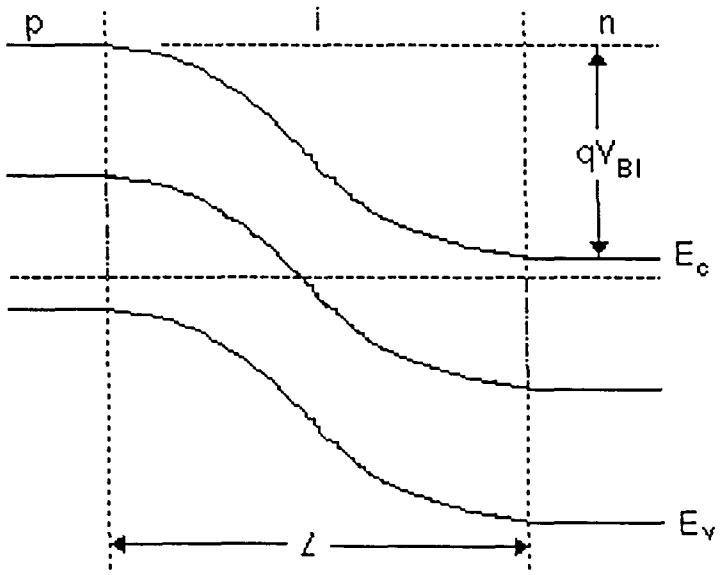

Figure 9. Short-circuit band diagram of p-i-n structure

built-in electric field falls faster with position into the i-layer in alloyed material. It can even reduce the field to zero near the middle of the i-layer. Also, increased DOS due to light degradation has a similar effect on the electric field. Holes generated at and beyond this low-field region depend on diffusion to get through to the p-i interface; and, as a result, often suffer recombination before they get there. Improvements to the i-layer structure can reduce this effect and are studied in detail in the next section and in the device optimization section.

F. Tandem Cells

Tandem cell structures are one way to overcome low electric fields in the middle of the i-layer.[13] The top of the cell of Figure 10 has a wide band gap i-layer, and collects most of the high energy photons. The layer is made thin (0.3μm), so the electric field is maintained at a high level, even if degradation

does occur. The bottom cell is made with narrower band gap material for collecting the lower energy photons. For high efficiency, the photogenerated currents must be equal in each cell. Thus, the bottom cell is slightly thicker than the top cell since sunlight has fewer low energy photons, and they travel farther before being absorbed.

The connection between the cells is achieved by doping the middle p- and n-layers very heavily so that a tunnel junction is formed. The increased complexity raises the production cost of tandem cells, but this can be offset by the increased efficiency from these structures.

Three cell tandem structures can increase the efficiency even further, but the added cost is often too high. Also, matching the currents from each layer becomes more difficult as the number of layers increases and sunlight conditions change, so two cell tandem structures are about the limit. If the bottom layer uses the doping structure proposed in the optimization section in chapter 4, the two cell tandem structure may be the most efficient and cost

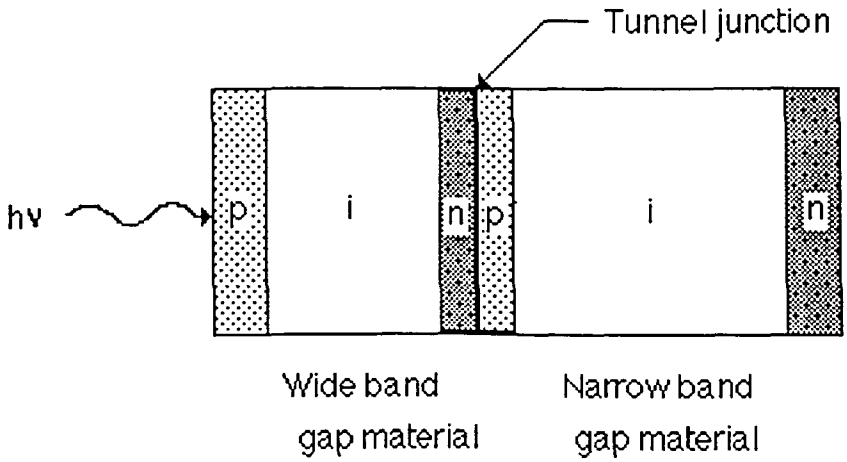

Figure 10. Schematic representation of a tandem solar cell

effective.

A further improvement to solar cell structures is to reflect light off the back of the device. The lowest energy photons produced by the sun can travel completely through even low band gap (1.5 eV) material, and are lost if there is no back reflection. Increasing the thickness of the i-layer would increase the absorption of these photons, but the electric field would drop too low to successfully collect the generated holes. A better method for collecting low energy light is to texture the back surface to increase its reflection coefficient. If the top surface is also textured, most of the photons become trapped in the i-layer until they are absorbed. This condition, shown schematically in Figure 11 is modeled in this simulation.

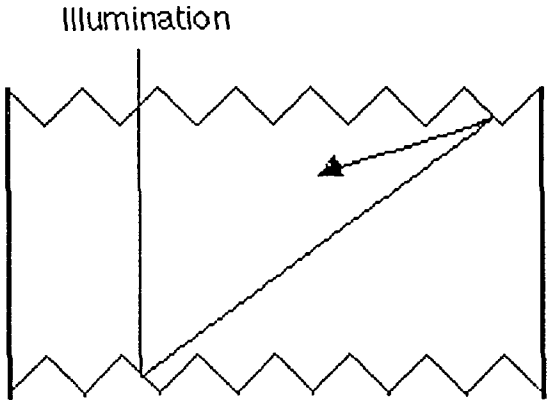

Figure 11. Low-energy photon reflection from the front and back surfaces of textured solar cell

III. DESCRIPTION OF THE MODEL

A. Electric Field Profile

The simulation of photogenerated carrier collection begins with a realistic solution for the non-uniform electric field profile in the i-layer. A typical electric field profile is shown in Figure 12. A high (10^5 V/cm), nearly constant field is always present at the p-i and i-n interfaces, but is reduced in a very short distance by the high DOS in the band tails.[5] When the DOS changes from band tails to deep level defects, the electric field falls more slowly. This model only computes the field in the middle of the i-layer up to the high interface fields, since this field changes under different band gaps and biasing conditions and has the greatest effect on efficiency.

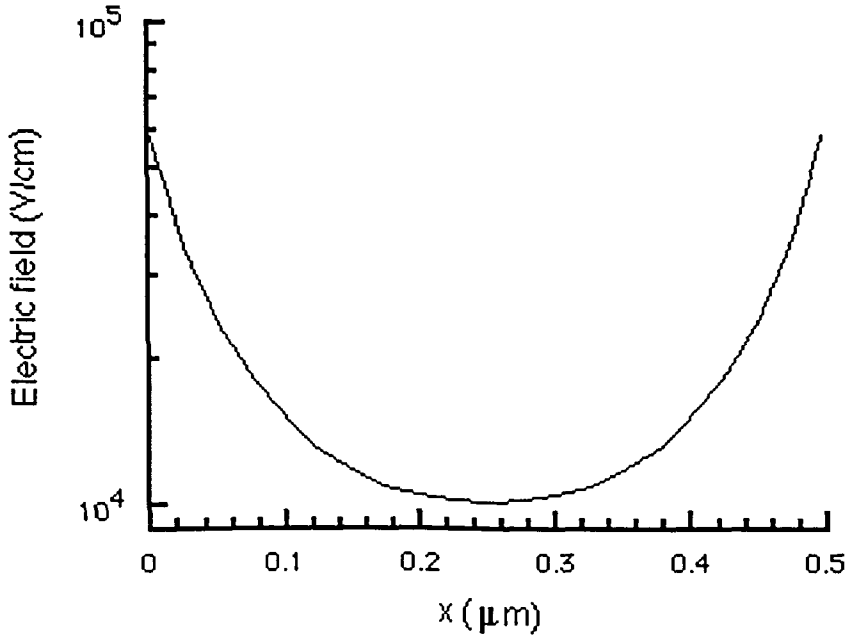

Figure 12. Typical i-layer electric field profile

The field can be found by solving the one-dimensional Poisson equation:

$$\frac{\partial \mathcal{E}}{\partial x} = \frac{\rho(x)}{\in} \qquad (6)$$

where $\mathcal{E}$ is the electric field, $\rho(x)$ is the space-charge density, and $\in$ is the dielectric constant of a-Si:H.

To find the space-charge density $\rho(x)$, the energy-dependent DOS:

$$g(E)=g_o \exp\left(\frac{E}{E_a}\right) \qquad (7)$$

is integrated over the energy from the fermi level to the position in energy of g_o, which is the area of the cross-hatched region in Figure 13. The position of g_o marks the transition from acceptor-like states found in the upper half of the band gap, to donor-like states in the lower half of the band gap, and is generally located near the middle of the gap. Then, for a junction with p-type or n-type material, band bending occurs in the i-layer as shown in Figure 13, and the donor-like states give up an electron as they move above the fermi level and become positively charged. These states are shown by the cross-hatched area in the left half of the i-layer in Figure 13.

The acceptor-like states of Figure 13 capture electrons in the right half of the i-layer, and become negatively charged. Since the value of g_o depends on the composition of the material, as explained in Chapter 2, its value will change

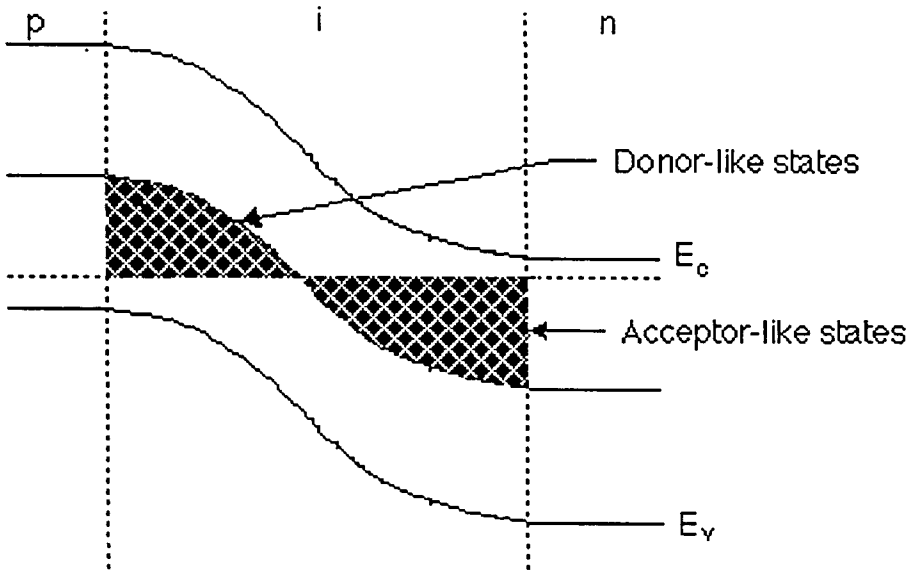

Figure 13. Band diagram showing occupied midgap defect states

throughout the i-layer when the band gap is graded. From experimental results, the value of g_o can be found directly from the value of the band gap by:

$$g_o(E_g)=C_1\exp(-C_2E_g) \qquad (8)$$

where E_g is the band gap, and C_1 and C_2 are experimentally derived.[14] Typical values for these parameters are 9.76×10^{22} $cm^{-3}eV^{-1}$ for C_1, and 10.5 eV^{-1} for C_2, which produce g_o values of about 10^{15} $cm^{-3}eV^{-1}$, and 10^{16} $cm^{-3}eV^{-1}$ for E_g=1.75 eV and 1.5 eV respectively.

Once g_o is determined for every position x in the i-layer, $\rho(x)$ is found from:

$$\rho(x) = qg_o\int_{E_f}^{E}\exp\left(\frac{E'}{E_a}\right)dE' + qN_t \qquad (9)$$

where N_t is a defect density that is only non-zero when simulating degraded conditions. The approximation for these defect states created by degradation is that they are at the center of the band gap and are of the same type as the other deep level states in that region. Then, the donor-like states are positive when they are below the fermi level and the acceptor-like states are negative when they are above the fermi level.

The analysis of $\rho(x)$ assumes a zero-temperature occupation probability for the defect states. In other words, when a state moves across the fermi level, it is immediately occupied. This approximation results in an occupation probability error on the order of kT/qE_a. The error is small when E_a is greater than kT/q, which it is by a factor of four or greater.

After the integral in equation 9 is evaluated, and $d\mathcal{E}/dx$ is converted to $\mathcal{E}d\mathcal{E}/dV$, Poisson's equation can be written as:

$$\mathcal{E}d\mathcal{E} = \left\{ \frac{qg_oE_a}{\in} \left[\exp\left(\frac{qV}{E_a}\right) - 1 \right] + \frac{qN_t}{\in} \right\} dV \qquad (10)$$

where qV was substituted for the energy E. Integrating and solving equation 10 for $\mathcal{E}$ results in:

$$\mathcal{E} = \sqrt{\frac{2g_oE_a^2}{\in} \left[\exp\left(\frac{qV}{E_a}\right) - 1 \right] + \frac{2q}{\in}\left[N_tV - g_oE_aV\right] + \mathcal{E}_o^2} \qquad (11)$$

where $\mathcal{E}_o$ is to be determined.

Substituting dV/dx for $\mathcal{E}$, and integrating produces the equation for the

energy qV at any position x:

$$x = \int_{o}^{V_f} \frac{dV}{\sqrt{\frac{2g_o E_a^2}{\epsilon}\left[\exp\left(\frac{qV}{E_a}\right) - 1\right] + \frac{2q}{\epsilon}\left[N_t V - g_o E_a V\right] + \varepsilon_o^2}} \qquad (12)$$

This equation is solved numerically for V and substituted back into equation 11 to obtain $\mathcal{E}(x)$.

There are two ways to determine the value of ε_o in equation 12. The method used in most computer models is to find ε_o by matching the electric fields at the p-i and i-n boundaries.

Another method can be used if the value of V_f shown in Figure 14 is known. Since qV_f in all biasing conditions is the energy between the fermi level and the position in energy of g_o, the value of V_f can be closely predicted from the value of the band gap and the position of g_o. Then, for V_a, the amount of biasing voltage, the value of V_f can be found from the following approximate relationship:

$$(qV_f/2) = \Delta E/2 - (qV_a/2) \qquad (13)$$

where V_a is the applied voltage and ΔE is the energy extent of the deep level defects.

Once V_f is determined, the integral in equation 12 can be solved for x with an estimated ε_o. Then, a new value of ε_o can be found by comparing the

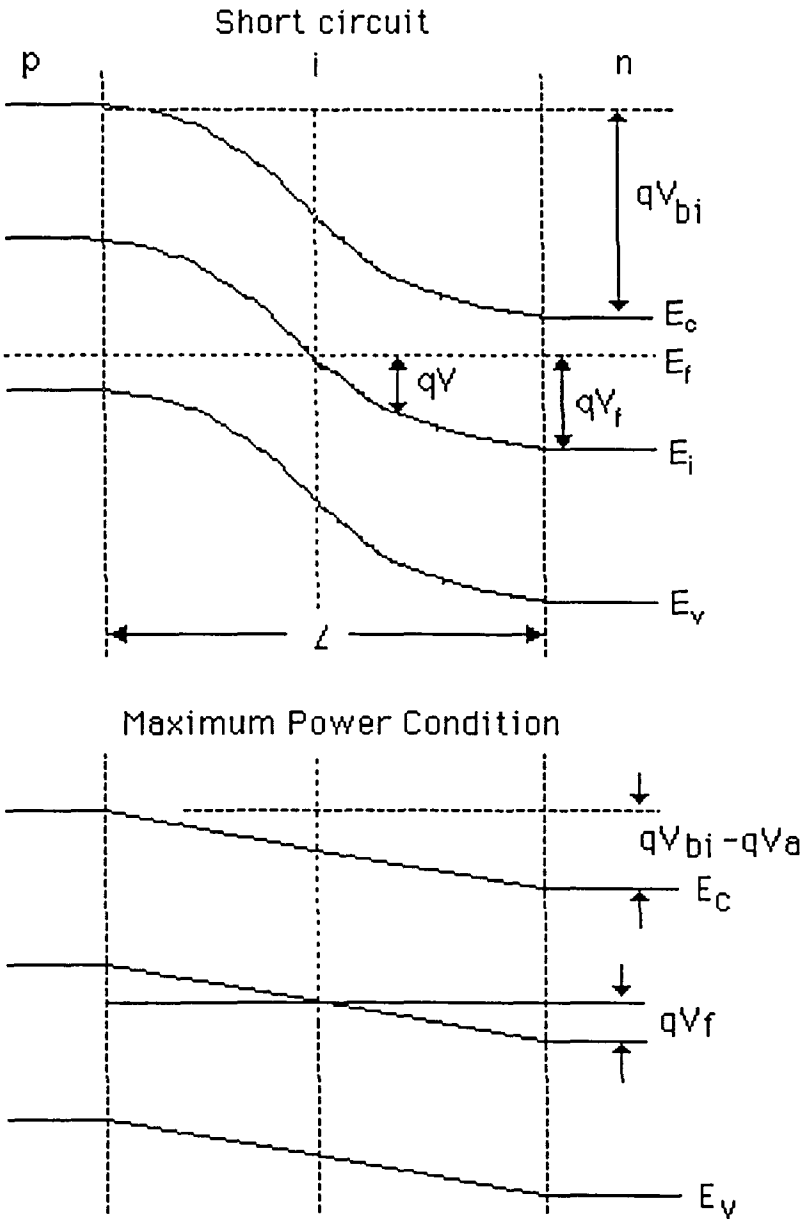

Figure 14. Band diagram of the p-i-n structure at short circuit and maximum power biasing conditions

value of x found from equation 15 to the total length of the i-layer; *L*. This process is repeated until the values of x and *L* are equal, then $\mathcal{E}(x)$ is completely and uniquely defined. If the band gap is different at the two ends of the i-layer, the position of $\mathcal{E}_o$ will not be at the center, but will be shifted toward the side of lower band gap, as shown in Figure 15.

To perform the integration in equation 12, a fortran program was written that uses a simple Simpson's quadrature routine. This method works well since V is a continuous, slowly varying function of x. The integrand is evaluated at a minimum of 100,000 points, resulting in a minimum of 30,000 points for $\mathcal{E}(x)$ with a relative error for the integration of less than one percent. The program for finding the electric field and the quantum efficiency is given in appendix B.

Additional hole diffusion fields due to a sloping valence band from a

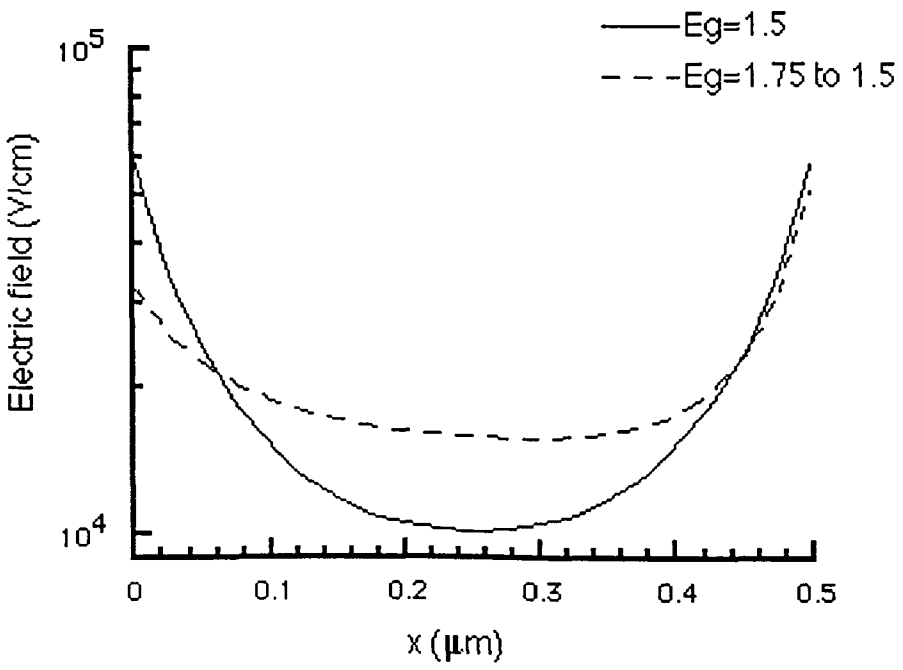

Figure 15. Electric field profiles of constant and linearly graded band gaps

graded band gap are added to $\mathcal{E}$ using $\mathcal{E}=d\Psi/dx$. At this point, only the hole fields are computed, since holes are the limiting carrier in amorphous material. In other words, if a hole is collected in the p-layer, the electron that was generated with the hole will also be collected.

B. Carrier Collection and Photogeneration

Once the electric field is found, the hole kinetics can be simulated using the concepts of Smith.[15] An effective diffusion length, known as the down-stream diffusion length L_d, can be found from :

$$\frac{1}{L_d} = \frac{1}{2L_p}\left[\left(\frac{\mathcal{E}}{\mathcal{E}_c}\right)^2 + 4\right]^{\frac{1}{2}} - \frac{\mathcal{E}}{2L_p\mathcal{E}_c} \qquad (14)$$

where L_p is the zero-field diffusion length, and $\mathcal{E}_c$ is a critical field defined by:

$$\mathcal{E}_c = kT/qL_p \qquad (15)$$

For a given density of holes Δp_o generated at some point in the i-layer, the hole density Δp at any distance x from that point can be found from:

$$\Delta p=\Delta p_o \exp\{-x/L_d\} \qquad (16)$$

The value of L_p depends on the density of defect states in the material. From

the definition of diffusion length and the fact that mobility is proportional to 1/g(E) in amorphous material, the following relationship is derived:

$$L_p = L_{po}\, g_o^{-1/2} \qquad (17)$$

where g_o can be found from equation 8 for any value of E_g, and L_{po} is on the order of 2000 $cm^{1/2}\, eV^{-1/2}$.[6]

The final step before computing the quantum efficiency is to determine the number of holes generated in the i-layer. The total number of ehps generated by photons is assumed to be equal to the number of photons absorbed. An expression for the number of ehps at any point in the i-layer can be derived from the definition for the absorption coefficient and is:

$$G = G_o\, \alpha(\lambda)\, \exp\{-\alpha(\lambda)x\}\, \{1-R(\lambda)\} \qquad (18)$$

where G_o is the incident photon flux and $\alpha(\lambda)$ is found from equations 2 and 4. $R(\lambda)$ is the reflection coefficient of the top surface of the cell, which can be made small with the addition of an anti-reflection coating.

C. Quantum Efficiency

Now the quantum efficiency can be computed at any given wavelength λ by:

$$QE(\lambda) = \frac{\#\text{ collected holes}}{\#\text{ incident photons}} = \int_0^L G(\lambda) \exp\left[\int_o^{x'} \left(-\frac{dx'}{L_d}\right)\right] dx \qquad (19)$$

where L is the length of the i-layer. Since $G(\lambda)$ and L_d are also functions of x if the band gap changes in the i-layer, this integral must be solved numerically. The absorption coefficient α is continuous over the entire length L since the band gap is continuous over L, so the integrals in equation 19 can be solved with a Simpson's quadrature routine. The integrand of the inner integral can be evaluated at each of the 30,000 data points found for $\mathcal{E}(x)$, for an overall relative error of three percent for all numerical methods.

This error is small in comparison to the fluctuations in experimental data, so the accuracy of the quantum efficiency simulation depends primarily on the accuracy of $g(E)$, $\alpha(\lambda)$, E_g, V_f and L_p. Also, the exact value of the electric field profile will depend on the number of charge carriers in the i-layer. These factors do not affect the results of this model since exact quantitative values are not the goal. The general trends in device efficiency will be accurately predicted by this method since all the approximations affect each device equally.

The quantum efficiency curves for various structures can be compared and device quality judged. For this report, the total area under the quantum efficiency curve will be calculated numerically and given as QET. This term represents an overall quantum efficiency when normalized to the range in incident wavelengths. QET is used to compare device efficiency for the various i-layer structures. The wavelength range utilized here is 400 to 800 nm, since higher wavelengths are not present in large quantities in sunlight, and lower

wavelengths are easily absorbed in all structures, so the quantum efficiency over these wavelengths provides the most information about the cell.

IV. COMPUTER SIMULATIONS AND RESULTS

A. Verification of the Model

To verify that the model accurately predicts the electric field profile, the parameters used by Hack and Shur in their complete model are used here, and the fields produced by each method are compared in Figure 16.[5]

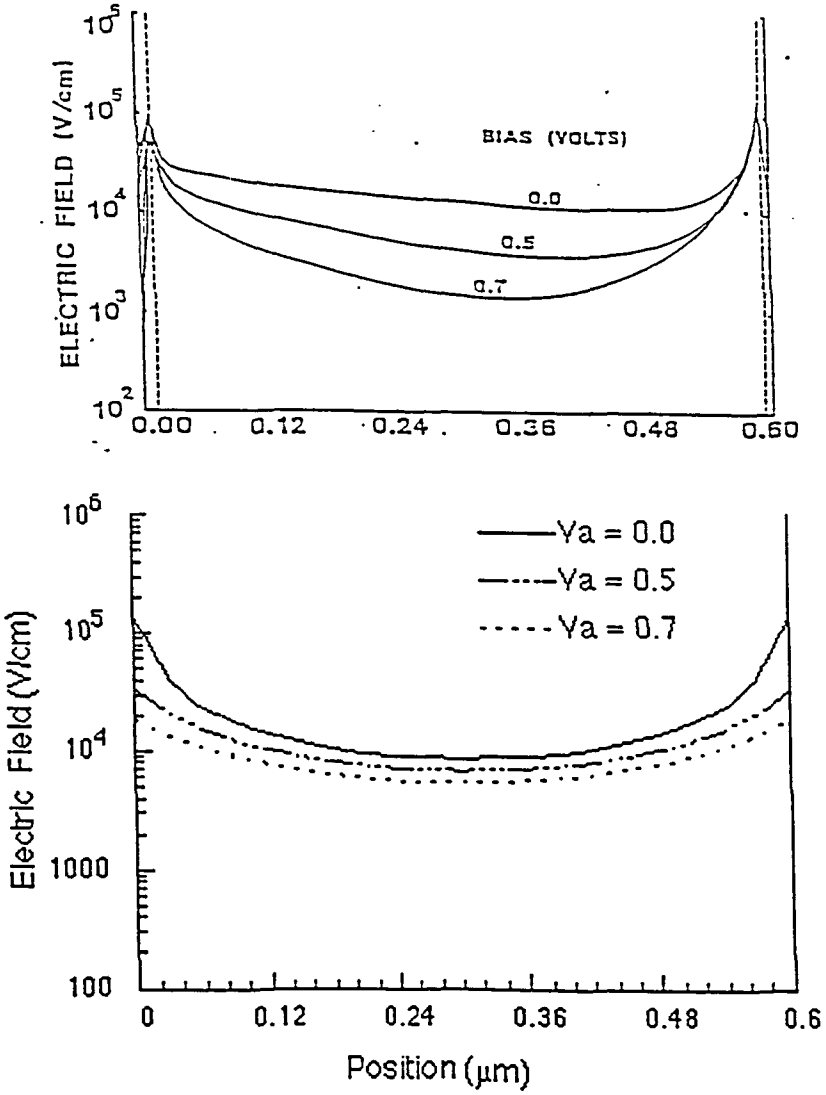

Figure 16. Electric field profiles from Hack and Shur (top), and this model (bottom)

As expected, the fields produced by the simplified approach do not maintain a constant interface value since the boundary conditions are not used, but this will not significantly alter the quantum efficiency since the charge carriers near the interface do not need high fields to be collected. The presence of charge carriers has a small effect on the value of the fields near the middle of the i-layer as seen in Figure 16, but the effects of biasing voltage are reproduced reasonably by the simplified approach and other effects can be studied as will be seen later in this section.

To verify that the model accurately predicts which device structures will have higher efficiencies; quantum efficiency and QET values for several previously reported structures are computed. These structures have band gap profiles shown in Figure 17.

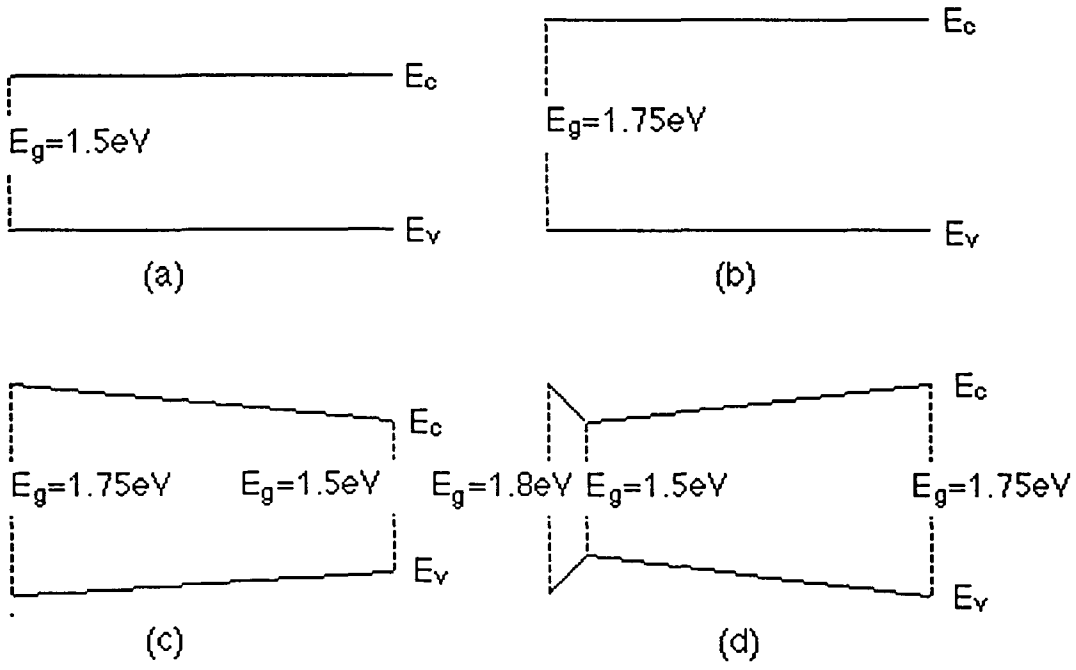

Figure 17. Band gap diagrams of the four structures used to test the model

The quantum efficiency and QET values for each of the structures is shown in Figure 18 with the same forward bias voltage and no material degradation (N_t=0). Structure (a) has a low, constant band gap with a high QET value due to its high overall absorption coefficient. This structure will not have a high open circuit voltage as outlined in Chapter 3, since the band gap is narrow. Since this is not modeled, it is simply noted, and devices with low interface band gaps will not be considered from now on, since high efficiency devices will have high open circuit voltages as explained earlier.

Structure (b) has a wide, constant band gap, and its QET value drops

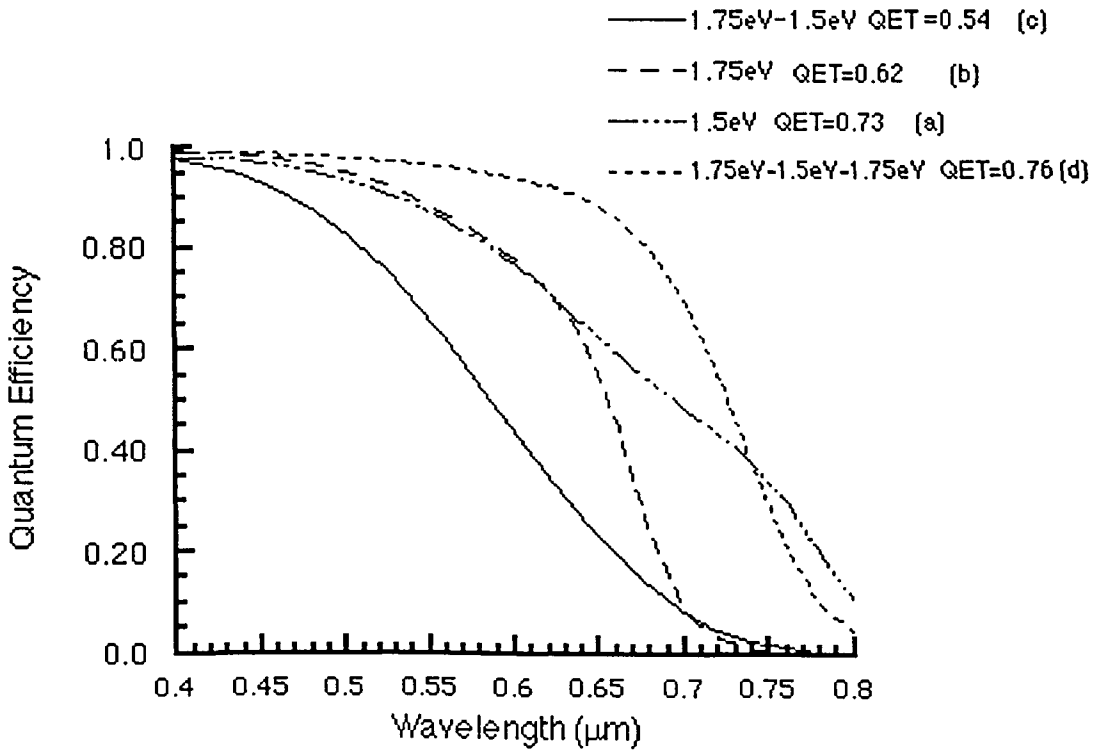

Figure 18. Quantum efficiency curves and QET values of structures a,b,c and d

dramatically from that of structure (a). As seen in Figure 18, low energy photons are not absorbed in this material, even after multiple reflections. The high value of open circuit voltage for this structure will be offset by its inability to absorb photons.

The absorption coefficients in structure (c) are higher than those in structure (b), since more low energy photons can be absorbed in the low band gap region at the back of the i-layer, but the fact that the band gap decreases from a high value at the p-layer to a low value at the n-layer means that the valence band is sloped in the wrong direction to assist in hole collection, resulting in even lower QET values than those for structure (b). So even though more carriers are generated in this structure, fewer are collected.

This fact suggests that structure (d) should be an improvement. The double graded structure has a wide initial band gap, a narrow band gap region for low energy photon absorption, and a sloping valence band that assists hole transport over the majority of the region. This structure's quantum efficiency and QET values are significantly better as seen in Figure 18.

These results are similar to those reported by Pawlikiewicz and Guha, and others, and sufficiently verify the accuracy of the model.[5,16-19] The structures shown in Figure 17 show the progression toward higher device efficiencies, but a closer look at the parameters controlling the value of QET should provide some insight into how further improvements can be achieved.

B. Optimization of Cell Efficiency

From the results of the verification section, it is clear that multiple band gap grading is necessary for high efficiency. Assuming that an i-layer has the

high interface band gap required for a high V_{oc}, and a low band gap region for low energy photon collection, the primary parameter controlling the quantum efficiency becomes the electric field. The two factors that reduce the electric field are applied bias and increased defect states due to degradation. This can be seen by comparing the quantum efficiency of structure (b) to the quantum efficiency for the same structure for various biasing voltages (Figure 19), and after light degradation produces charged midgap defect states with a density of N_t (Figure 22). The electric fields for various values of biasing voltage V_a and defect density N_t are compared in Figures 20, 21, and 23. The characteristic parameter values used for the structure (b) material are listed in Table 1.

The electric field profiles in Figure 20 decrease with increasing forward bias, but remain sufficiently high to maintain carrier drift in the middle of the i-layer, and the collection efficiency will remain high for this structure When the

Table 1. Set of realistic parameter values used in the model.

Band gap: $E_g = 1.75$ eV
Minimum DOS: $g_o = 2x10^{15}$ cm^{-3} eV^{-1}
DOS energy slope: $E_a = 100$ meV
Hole diffusion length: $L_p = 5000$ A
Built-in voltage: $V_{BI} = 1.1$ V
Length of i-layer: $L = 0.5$ μm
Absorption coefficient prefactor: $B = 750$ cm$^{-1/2}$ eV$^{-1/2}$

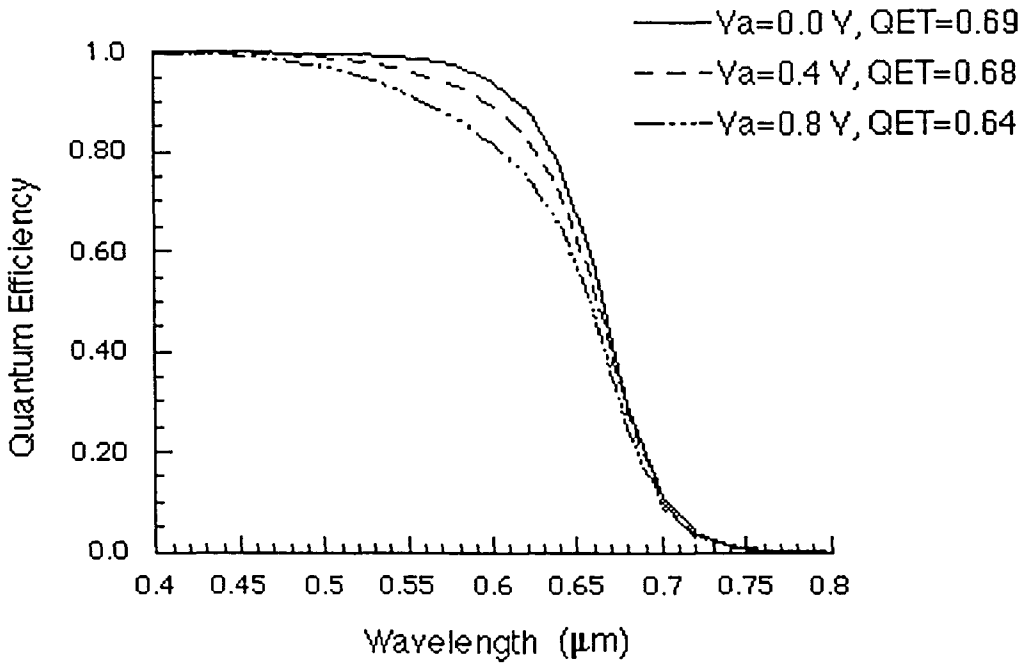

Figure 19. Effects of forward bias on the quantum efficiency for structure b with Nt=10^{16} cm^{-3} degradation defect states

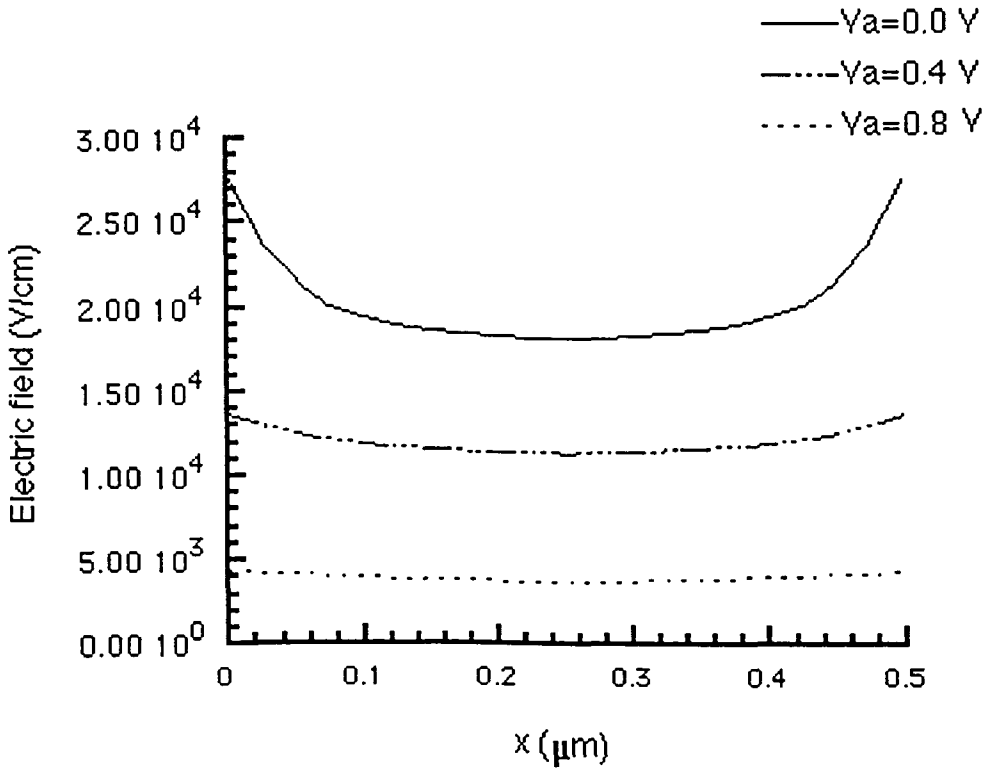

Figure 20. Electric field profiles of structure b with Nt = 0 cm^{-3}

degradation defect density begins to increase, though, the electric field can fall to zero in the middle of the i-layer as shown in Figure 21.

The linearly decreasing electric field profiles in Figure 21 show that the large constant value of N_t dominates the charge density in the i-layer when degradation occurs. Biasing at the maximum power point (Va=0.8) reduces the electric field to zero for the majority of the i-layer, so the quantum efficiency and QET values will be much lower as shown in Figure 22.

Figure 21 shows that the electric field in a degraded structure falls to zero even for open circuit conditions. The QET values are much lower than the undegraded material as expected. The middle region of the i-layer has no band

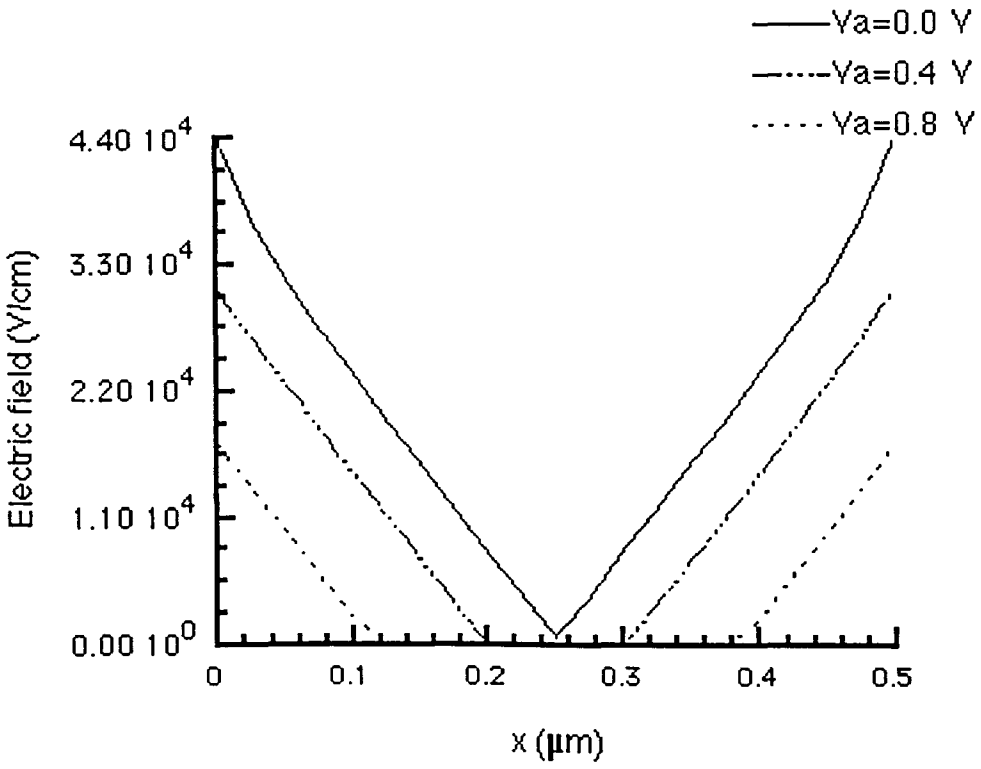

Figure 21. Electric field profiles of structure b under increasing bias voltage Nt=10^{16} cm^{-3}

bending at all, so collection of holes generated at or beyond this region depends purely on diffusion similar to the simple p-n junction cell. Decreasing the length of the i-layer would reduce the flat-band region in degraded material, and is the reason for the increased efficiency in tandem cell structures as explained in Chapter 2.

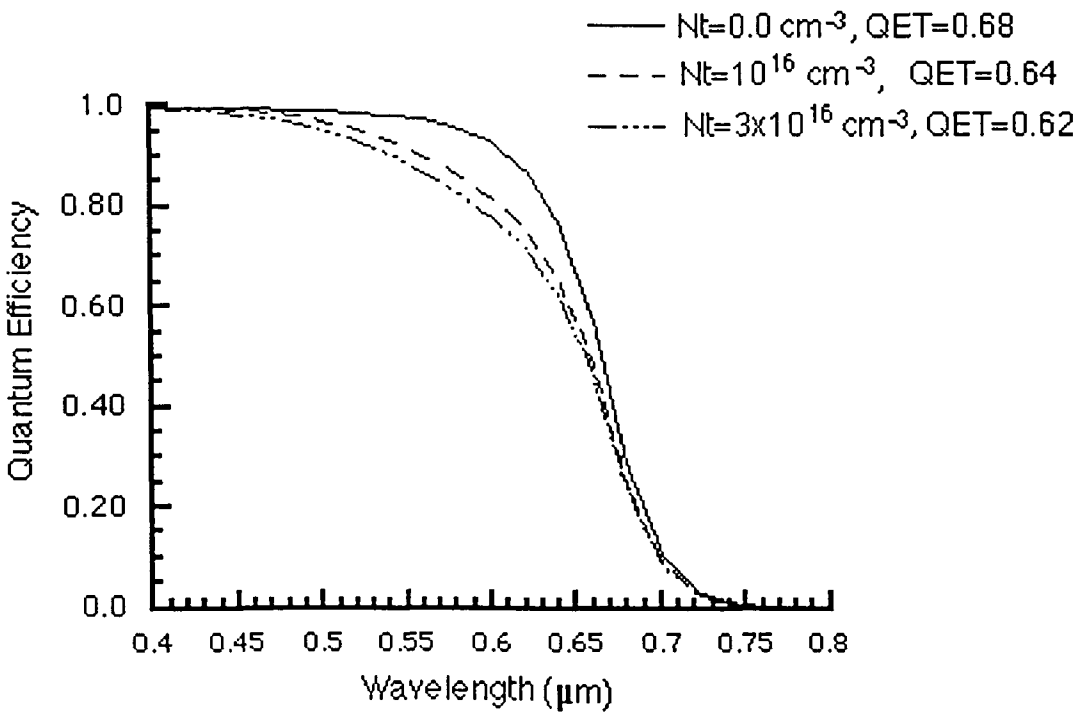

Figure 22. Quantum efficiency curves and QET values of structure b with increasing levels of degradation densities and biased at the maximum power point (V_a=0.8 V)

Since it is not practical to have more than two cells in tandem, the bottom cell must be made thick enough to capture most of the low energy photons, and may reach the flat band condition for large N_t. The electric field profiles of structure (b) for various degradation levels are shown in Figure 23, with biasing

at the maximum power point. The values of N_t used are typical of amorphous silicon, so a large zero-field region is present in all but the undegraded material.

Since an insufficient electric field causes large reductions in the quantum efficiency, new structures or materials that do not degrade must be found if higher efficiencies in thick material are to be realized. The new growth process in appendix A is one step along this direction, and the following analysis is another.

If a minimum carrier collection efficiency for photogenerated ehps is chosen, the electric field required to produce this efficiency can be computed. Maintaining the electric field above this optimum collection field value ($\mathcal{E}_c$) will ensure that carrier movement is a drift process. The collection field shown in Figure 23 will produce 95 percent collection of all photogenerated holes.

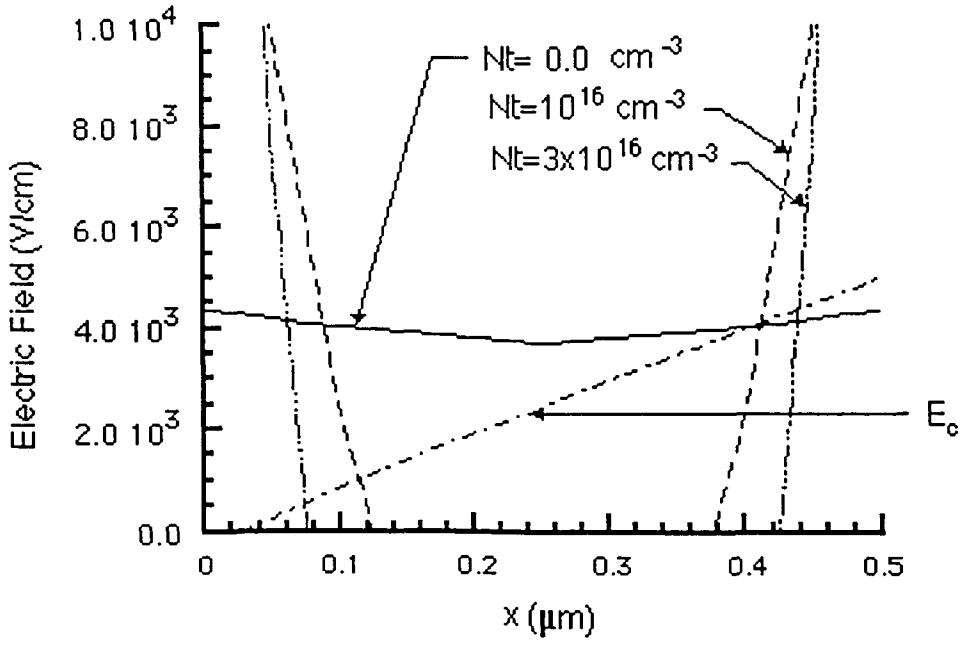

Figure 23. Electric field profiles of structure b with increasing levels of degradation density. Also shown is the constant collection efficiency field

Electric field values higher than ε_c do not increase the quantum efficiency very much, but fields lower than ε_c quickly reduce the quantum efficiency. Figure 23 shows that the electric field falls far below the collection field in the middle of the i-layer as the material becomes degraded. The method for increasing the electric field closer to the collection field value is to add hole diffusion fields by grading the band gap. There is only a limited amount of band gap grading that can be done since the band gap should not be lower than 1.5 eV or higher than 1.8 eV as mentioned in Chapter 3. The hole field can be increased near the middle of the i-layer, where it is needed the most by only grading the band gap in that region. The back region of the i-layer has a high built-in field, so does not require band gap grading, and the front region must have the high initial band gap graded to low band gap as usual. The structure shown in Figure 24, first proposed by Dalal, only has band gap grading where

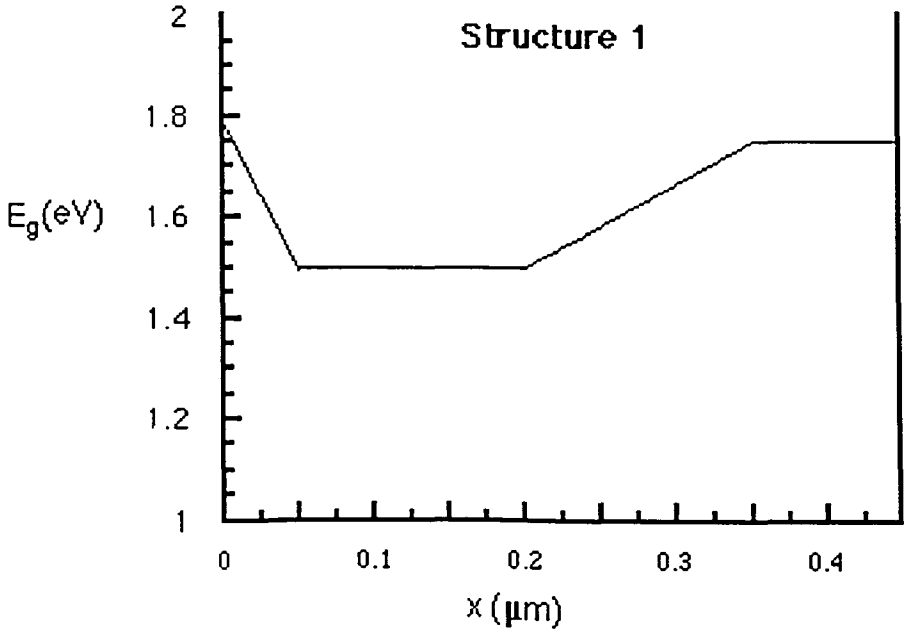

Figure 24. Graded band gap profile for increased efficiency

needed.[4] The quantum efficiency and QET values shown in Figure 25 are an improvement over even the double-graded structure.

The highest QET value for the double graded structure with no degraded states found with this model was 0.76 while the QET value for structure 1 also

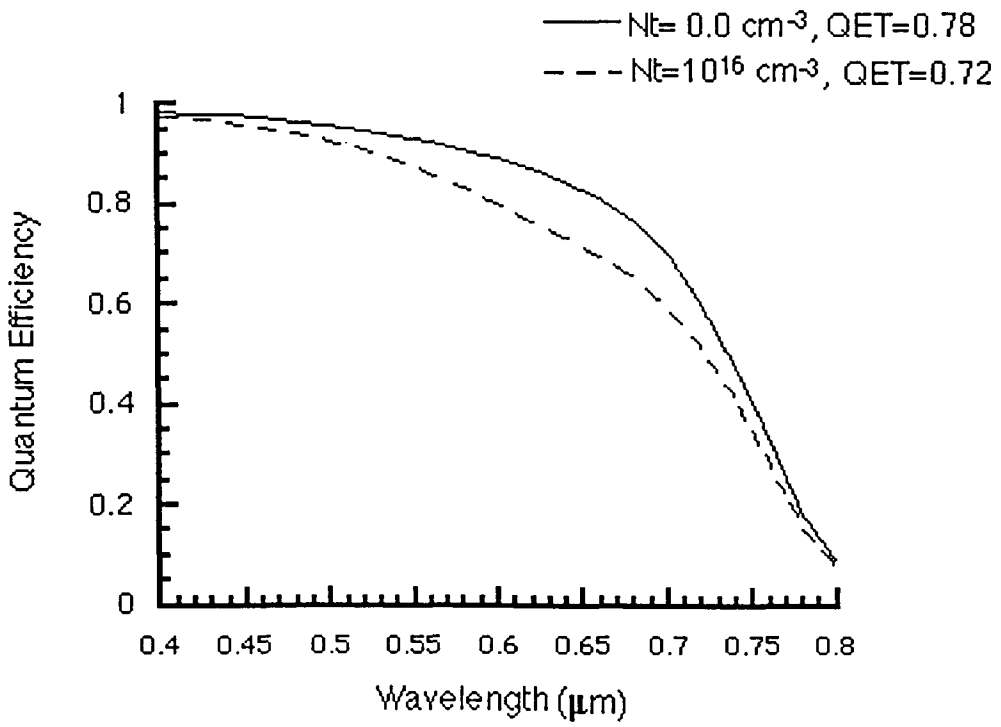

Figure 25. Quantum efficiency curves and QET values for two levels of degradation density for structure 1

with no degraded states is 0.78. The addition of degraded states lowers the QET value to 0.72, suggesting that if a known value of degraded states will be present in a material, the optimized structure must be modified.

The collection field ε_c for the improved structure, shown in Figure 26, increases quickly in the low band gap region because of the low transport parameters typical of alloyed material. Thus, it is necessary to limit the extent of

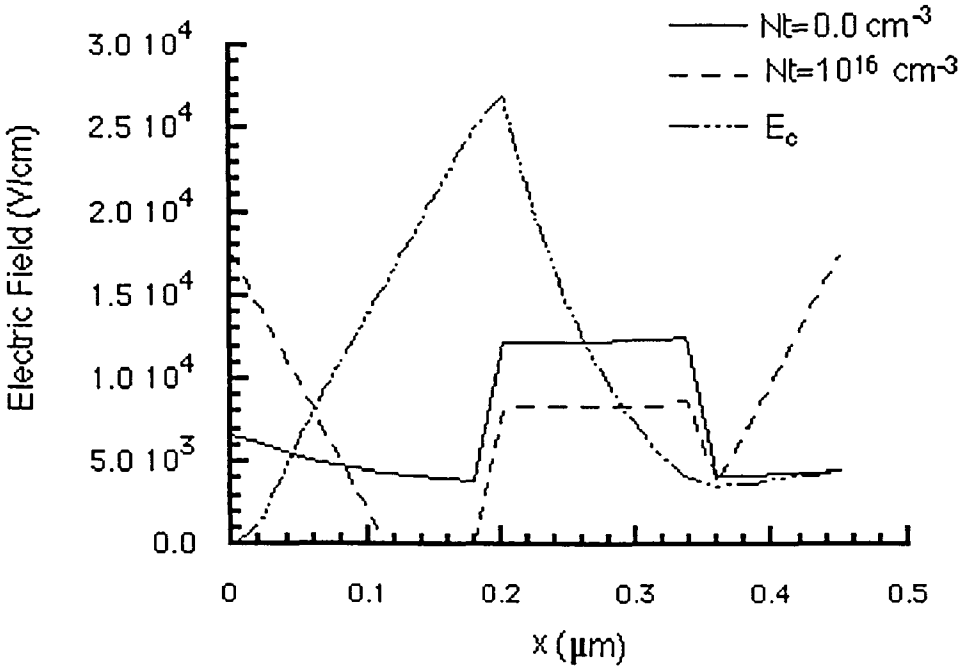

Figure 26. Electric field and constant collection field profiles in structure 1

the low band gap region to only that amount required to capture most of the low energy photons. Also, this region should be kept as near to the p-i interface as possible. Finding the right combination of band gap grading and light absorption can be difficult, and emphasizes the value of a good computer model.

If it is known that a material degrades to a stable value of N_t, the structure of Figure 24 can be optimized for this condition. The grading should start near the position where the built-in field falls below ε_c, and end near the same point at the back of the i-layer. The region before the grading begins will still have the high interface fields, so is kept at the low value required for low energy photon absorption. Since the value of N_t can be different for each particular material

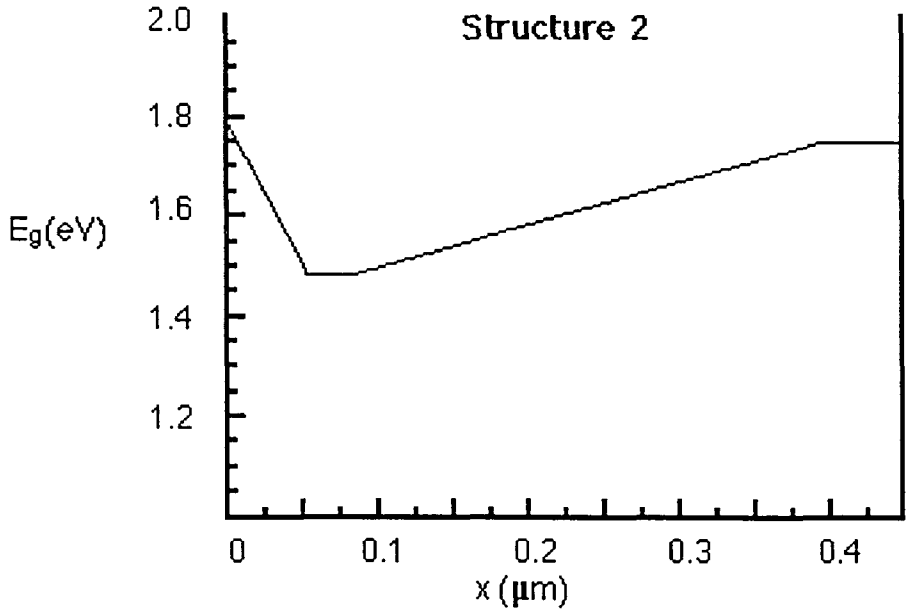

Figure 27. Optimized band gap structure for a heavily degraded solar cell

fabrication system, a single high value is chosen here to show how the model is used to find the highest efficiency structure. The optimized structure for $N_t=3x10^{16}$ cm^{-3} is shown in Figure 27.

The quantum efficiency and QET values do increase for this idealized structure as seen in Figure 28, even with a greater defect density than in structure 1. Once the value of N_t is determined for a particular growth system, a structure similar to structure 2 can be made. The length of the i-layer *L* will depend on if the structure is used in a tandem or alone.

If the cell is to be a single layer, the optimum length can be found with this model using high back reflection coefficients. The length with the highest efficiency for a structure similar to structure 2 is around 0.55 μm. If the cell is to be the bottom layer of a tandem, the length must be made to produce the same

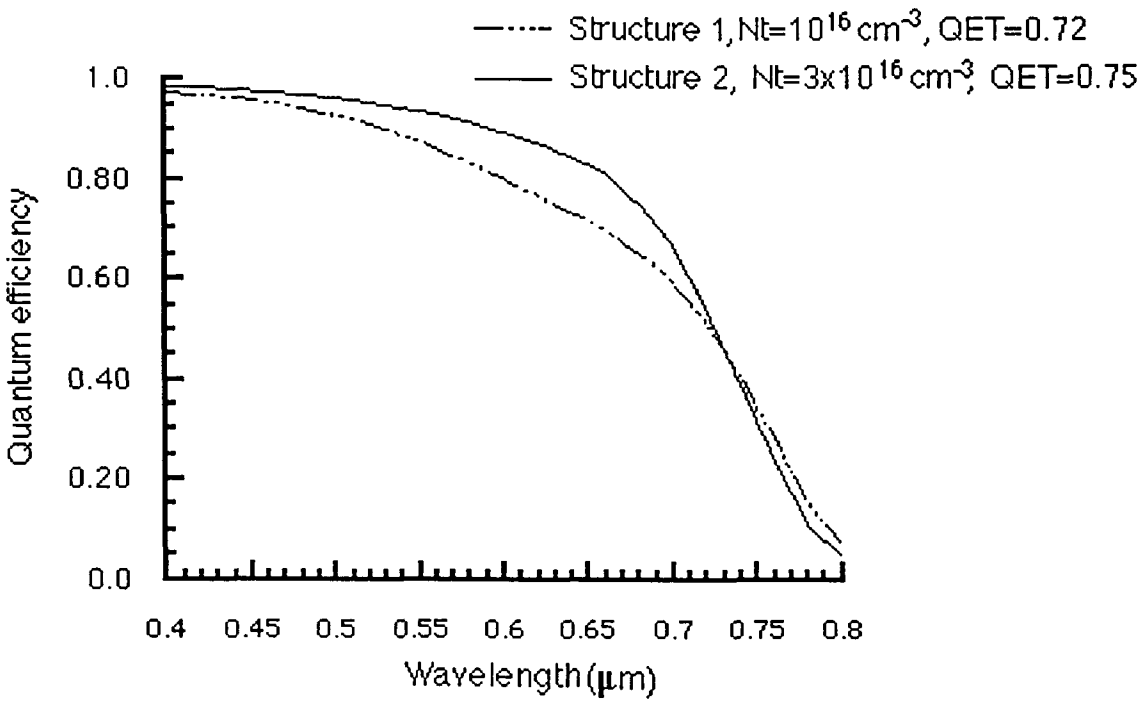

Figure 28. Quantum efficiency curves for structures 1 and 2 at V_a=0.8 V

photocurrent as the top layer.

The quantum efficiency curves of Figure 28 behave exactly as expected since the higher fields present in structure 2 allow greater carrier collection for almost the entire wavelength range. The only part of the spectrum that suffers a decrease in carrier collection is the very top end. The low energy photons are not as easily absorbed in structure 2 since there is less low band gap material.

The electric field profile shown in Figure 29 for the idealized structure comes closer to $\mathcal{E}_c$ throughout the i-layer. Since the value of collection efficiency for computing $\mathcal{E}_c$ was arbitrarily chosen, it is not necessary for the electric field to be above $\mathcal{E}_c$ everywhere. It is necessary, though, to stay

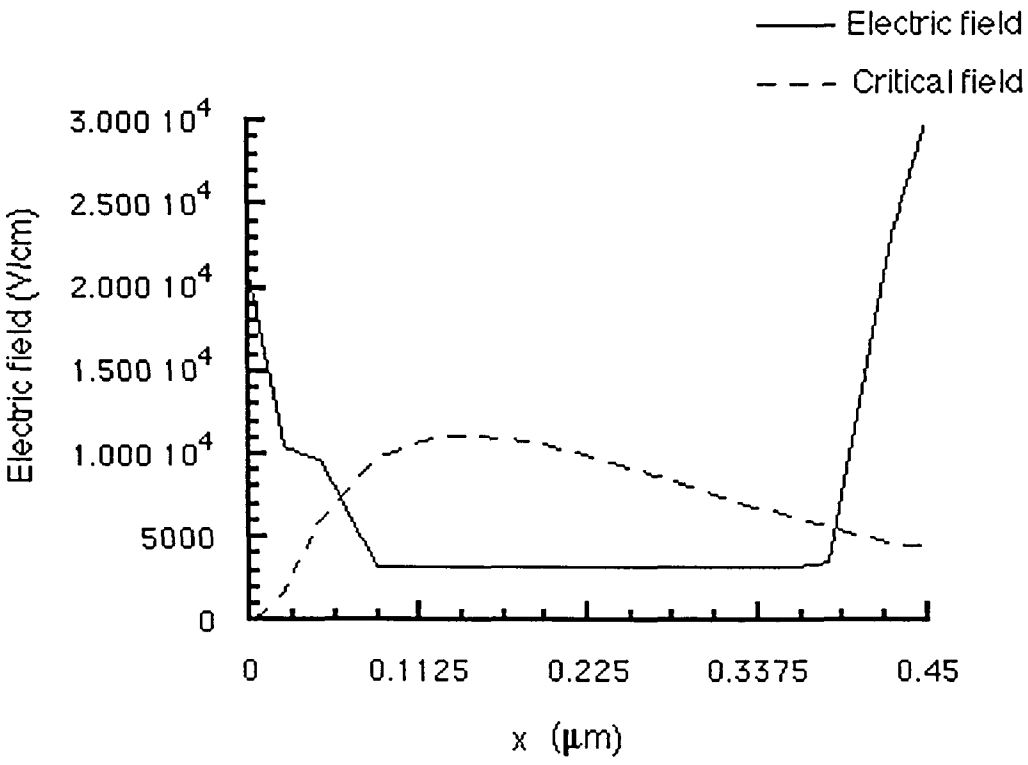

Figure 29. Electric field and constant collection field profiles in the structure 2

reasonably close to it as the fields in Figure 29 do to maintain high efficiency.

The only way to further increase the efficiency by band gap grading is to see if the slightly reduced hole field of less band gap grading is offset by the increased absorption from a larger, low band gap area. As the slope of the band gap is decreased for higher absorption, the value of QET , as shown in Table 2, decreases for a cell with high back reflection coefficients, showing that maintaining high fields is more important than increasing the absorption. This is not true for a cell without high back reflection coefficients. The larger low band gap area now results in a higher QET value for this condition, showing that absorbing the lower energy photons is more important than maintaining high

Table 2. Comparison of QET values for structures with low and high back reflection coefficients, and long and short low band gap areas.

Structure	Description	QET
1	short low band gap area, high electric field, high back reflection coeff.	0.763
2	long low band gap area, low electric field, high back reflection coeff.	0.761
3	short low band gap area, high electric field, low back reflection coeff.	0.660
4	long low band gap area, low electric field, low back reflection coeff.	0.665

electric fields. Thus, if texturing or providing a dielectric stack to produce high back reflection coefficients is not possible or practical, the design of such a cell will be different when optimizing the efficiency. All of the structures used to produce the values in Table 2 have a degradation density of $N_t = 10^{16}$ cm^{-3} and are biased at the maximum power point of Va = 0.8 V.

The method outlined here to optimize the efficiency of a solar cell with a particular degradation density, forward bias voltage and midgap state density can be used for any growth system once these parameters are known. As explained, the quantitative results will only be estimates, but the model allows for the design of the optimum band gap profile for a particular growth system.

V. CONCLUSIONS

The unique properties of amorphous silicon can be successfully modeled by the approach presented here. The flexibility of the analysis allows the freedom of design necessary for efficiency optimization, rather than being tailored to a specific device structure. All the parameters affecting carrier generation and collection are included in the model. The problem of device degradation is modeled and structures that can minimize its effects are proposed.

The electric field profiles produced by the model are sufficiently close to those found by others using a complete analysis including boundary conditions and charge carriers showing that the method used here is a valid approximation. It is also validated by reproducing experimental reports of several device structures by comparing the quantum efficiency of each device. The simplified approach presented here allows for the detailed study of a few of the main parameters controlling device efficiency, which leads to ways to improve the device structure. Then the model is used to guide the design of a new band gap grading structure for the i-layer of a p-i-n solar cell.

The new structures shown by the model to have increased efficiency can be optimized for the characteristics of a particular fabrication system. The system outlined in appendix A is part of an on-going effort to produce solar cell devices using these new types of structures. When the increased stability of this fabrication system is combined with an optimized device structure, the product may become a cost effective alternative to fossil fuels.

References

1. Catalano, A., Arya, R. R., Bennett, M., Yang, L., Morris, J., Goldstein, B., Fieselman, B., Newton, J., and Wiedeman, S., "Review of progress on a-Si alloy solar cell research." Solar Cells, vol. 27, p. 25-37, 1989.

2. Dalal, V.L., and Alvarez, F., "Minority carrier transport in depletion layers of n-i-p a-Si:H solar cells." Journal De Physique, Supplement C4, vol. 42, p. 491-494, October 1981.

3. Crandall, R.S., "Modeling of thin film solar cells: uniform field approximation." Journal of Applied Physics, vol. 54, no. 12, Dec. 1983.

4. Dalal, V. L., Moradi, B., and Baldwin, G., "Design considerations for stable amorphous silicon solar cells" Amorphous Silicon Materials and Solar Cells, Stafford, B., ed., American Institute of Physics, New York, p. 298-305, 1991.

5. Hack, M., and Shur, M., "Physics of amorphous silicon alloy p-i-n solar cells." Journal of Applied Physics, vol. 58, no. 2, p. 997-1020, July 1985.

6. Madan, A., and Shaw, M. P., The Physics and Applications of Amorphous Semiconductors. Academic Press, San Diego, 1988.

7. Mott, N. F., and Davis, E. A., Electronic Processes in Non-Crystalline Materials, Clarendon Press, Oxford, 1979.

8. Spear, W. E., and LeComber, P. G., "Investigation fo the localized state distribution in amorphous Si films." Journal of Non-crystalline Solids, vol. 8-10, p. 727, 1972.

9. Hama, S. T., Okamoto, H., Hamakawa, Y., Matsubara, T., "Hydrogen content dependence of the optical energy gap in a-Si:H." Journal of Non-crystalline Solids, vol. 59-60, p. 333, 1983.

10. Staebler, D. L., and Wronski, C. R., "Reversible conductivity changes in discharge-produced amorphous Si." Applied Physics Letters, vol. 31, no. 4, p. 292-4, Aug. 1977.

11. Adler, D., "Defects and density of localized states." Semiconductors and Semimetals, Pankove, ed., Academic Press, Part A, vol. 21, Chapter 14, New York, 1984.

12. Dalal, V. L., "A comprehensive model for photo-degradation in a-Si:H." Stability of a-Si Materials and Devices, Stafford, B., and Sabinsky, E., eds., American Institute of Physics, New York, p. 249-255, 1987.

13. Shur, M., Physics of Semiconductor Devices, Prentice Hall, New Jersey, 1990.

14. Hegedus, S. S., and Fagen, E. A., "Characterization of a-Si:H and a-(Si,Ge):H p-i-n and Schottky junctions by admittance circuit modeling." to be published in IEEE Transactions on Electron Devices.

15. Smith, R. A., Semiconductors, p. 184-8, Cambridge University Press, New York, 1978.

16. Pawlikiewicz, A. H., and Guha, S., "Numerical modeling of an amorphous-silicon-based p-i-n solar cell." IEEE Transactions on Electron Devices, vol. 37, no. 2, Feb. 1990.

17. Misiakos, K., and Lindholm, F. A., "Analytic and numerical modeling of amorphous silicon p-i-n solar cells." Journal of Applied Physics, vol. 64, no. 1, July 1988.

18. Swartz, G. A., "Computer model of amorphous silicon solar cell." Journal of Applied Physics, vol. 53, no. 1, Jan. 1982.

19. Guha, S., Yang, J., Pawlikiewicz, A. H., Glatfelter, T., Ross, R., and Ovshinsky, S. R., "Band gap profiling for improving the efficiency of amorphous silicon-alloy solar cells." Applied Physics Letters, vol. 54, no. 23, p. 2330, 1989.

20. Tsai, C. C., Anderson, G. B., Thomson, R., and Wacker, B., "Control of silicon network in plasma deposition." Journal of Non-crystalline Solids, vol. 114, p. 151-3, 1989.

21. Dalal, V. L., Knox, R., Kandalaft, N., and Baldwin, G., "Growth and properties of amorphous silicon films grown using pulsed-flow reactive beam epitaxy." Proceedings of 22nd. IEEE PVSC, 1991.

ACKNOWLEDGEMENTS

I would like to take this opportunity to thank Dr. Dalal for his generous help in completing this project and throughout my graduate school career. I would especially like to thank him for securing the Department of Education fellowship that has made my attendance here possible.

I would also like to thank Neil Johnson and the Center for Non-destructive Evaluation for allowing me to use their computation facilities, which greatly facilitated this research. Thanks also go to Dr. Gary Tuttle, Dr. Howard Shanks, and Dr. Stan Burns, my graduate committee members, for their time and valuable suggestions. Finally, I would like to thank my friends Behnam Moradi, Nabeeh Kandalaft and Er-Xuan Ping, all of whom have made graduate school more enjoyable for me with their friendship.

Special thanks go to my wife Laura. Her love and understanding throughout the many late nights and frustrations have allowed me to reach goals I never thought I would attain. Her own goals have been delayed while I attempt to complete mine, and I only hope that I can do the same for her in the future.

APPENDIX A: STABLE a-Si:H FABRICATION

The standard a-Si:H growth process by gas phase decomposition of SiH_4 leads to non-uniform Si deposition. Spikes of SiH_3 can grow on the surface, leaving voids in the between the spikes. This non-uniformity leads to material instability, since the incoming photon energy can facilitate carrier trapping in these voids.[11]

A deposition process that removes the voids during growth will have greater stability, and is the goal of the process described here. Microwave Electron-Cyclotron-Resonance (ECR) plasma deposition offers a way to control the growth chemistry on the surface during deposition. It has been shown that if energy is supplied to the growing surface only, the SiH_3 spikes are broken up without breaking weak bonds deeper in the amorphous system.[20] It is not desirable to break any of the weak bonds deeper in the material since this increases the defect density.

A high density of H or F ions bombarding the growing surface is one way to provide energy to the surface. These ions etch the surface by removing the poorly bonded Si in the SiH_3 spikes, leaving behind a vacant site for more perfect bonding. The ECR system provides such an ion bombardment and has resulted in more stable amorphous material.[21] The schematic representation of an ECR deposition system is illustrated in Figure 30.

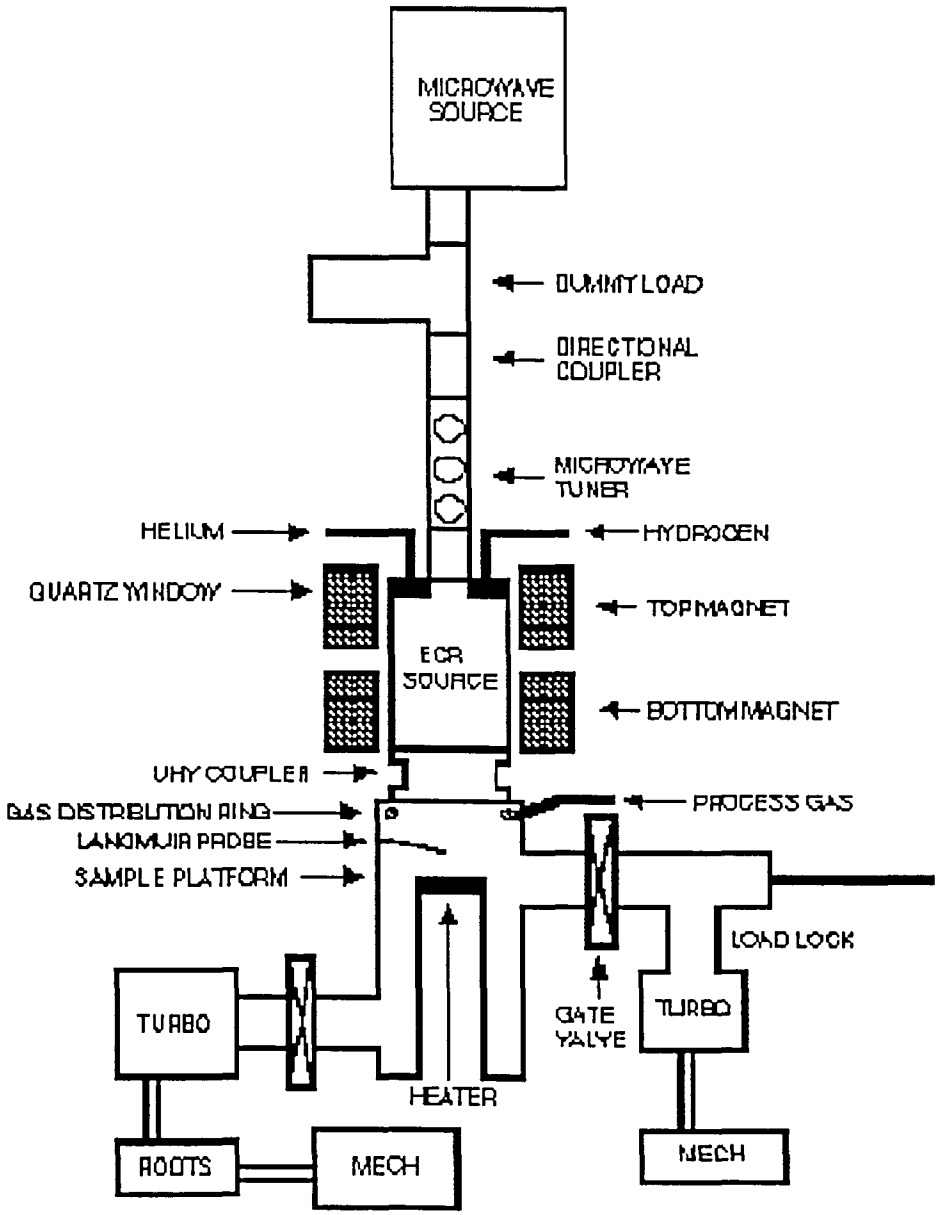

Figure 30. Schematic diagram of the ECR system

APPENDIX B: COMPUTER PROGRAM

```
      PROGRAM QEPIN
C
C     Purpose  Solve Poisson's equation for the electric field
C              as a function of position in the i-layer of a
C              graded band gap p-i-n junction solar cell, and
C              compute the quantum efficiency
C
C     Description
C              The method used is Simpson's rule quadrature
C              for the electric field and quantum efficiency
C              integrals as given in the text
C              When the value of Go is changing with position,
C              the i-layer is broken into 50 subintervals of
C              constant Go
C     Input parameters
C     LENGTH --> (real) length of the i-layer in cm
C     V1 ------> (real) char. energy slope (#/cm^3 eV)
C     EG ------> (real) initial band gap (eV)
C     EG2 -----> (real) final band gap (eV)
C     VEND(N) -> (real) ending voltage at each junction (V)
C     NT ------> (real) degraded defect density (C/cm^3)
C
C     Note: this program should be altered to accept
C              multple band gap grading

      INTEGER TEST,I,J,K,S1,S2,CHECK,L,NI,NIH,NIL,
     +     S(1000),N,FLAT,M,STOP
      PARAMETER (S1=2,S2=100,G1=-10.51237884,G2=52.93543891)
      REAL INCREASE,STEP,FACTOR1,FACTOR2,
     +  K2,V,QE,LENGTH,TEMP1,TEMP2,
     +  NT,MUTAU(555000),X,E,ALPHA1,ALPHA2,
     +  TERM,DIFF,EO2(S1,S2),VEND(S1),
     +  LAST(S1),XEND(S1,S2),TOTAL(S1),
     +  HNU,LAMDA,XE(555000),EX(555000),
     +  EG,ESTART,VSTART,XSTART,EOSTART2,
     +  ET(555000),XD(555000),XSTEP,XTEST,
     +  GO,V1,A(S1,S2),INNER(555000),
     +  DELX,DELY,B,SLOPE,HOLD,QET,VX(555000),
     +  VT(555000),VY(100000),QEW,LPC(555000)
     +  C3,C4,C5,TOTPROBC(100000),XPERM(100000)
     +  VSTEP,TOTLENGTH,ADD,BETA1,BETA2,VW(100000),
     +  HOLD2,LP(555000),EG2,EXADD,EGADD,GAP(100000),
     +  GAPC(100000),INNERC(100000),MUTAUC(555000),
     +  G1,G2,GO1,GO2,EC,MIN,ALPHAX,DALPHAX,D,C1,C2,
     +  TEMP3,C6,XB(55500),PROB,TOTPROB(0:10000),
     +  EAMB(50000),GAP2,GAP3,TOTPROBPERM(100000)
C
C
      READ(5,*)LENGTH,V1,EG,EG2
      TOTLENGTH=LENGTH
      WRITE(6,*) 'Length of i-layer: ',LENGTH*1.0E4
      WRITE(6,*)' Bandgap = ',EG,' To ',EG2
      SLOPE=(EG2-EG)/TOTLENGTH
```

```
      B=EG
      IF (SLOPE.EQ.0.0) THEN
              XEND(1,1)=1.0
              XEND(2,1)=1.0
              GO=EXP((G1*EG)+G2)
              WRITE(6,*)'Go = ',GO
              A(1,1)=2*1.6E-19*GO*V1/(12.*8.854E-14)
              A(2,1)=A(1,1)
              READ(5,*)VEND(1),VEND(2)
              FLAT=1
              GOTO 1
      END IF
      FLAT=-1
      XSTEP=TOTLENGTH/100.0
      DO I=1,2
              X=0.0
              K2=TOTLENGTH/2.0
              IF (I.EQ.1) THEN
                      WRITE(6,*) 'For p+ side '
              ELSE
                      WRITE(6,*) 'For n+ side '
              END IF
              READ(5,*) VEND(I)
              WRITE(6,*) 'Ending voltage = ',VEND(I)
              DO J=1,50
                      XEND(I,J)=X+XSTEP
                      GO1=EXP((G1*(SLOPE*K2+B))+G2)
                      K2=K2+(XSTEP*(-1.0)**I)
                      IF (K2.LT.0.0) K2=0.0
                      IF (K2.GT.TOTLENGTH) K2=TOTLENGTH
                      GO2=EXP((G1*(SLOPE*K2+B))+G2)
                      GO=(GO2+GO1)/2.0
                      GO=1.E16
                      A(I,J)=2.*1.6E-19*GO*V1/(12.*8.854E-14)
                      X=X+XSTEP
              END DO
              WRITE(6,*)' Go =',GO,' at x =',K2*1.E4
      END DO
      XEND(1,50)=1.0
      XEND(2,50)=1.0
1     READ(5,*) NT
      WRITE(6,*)'NT = ',NT
      EXADD=0.0
      XSTEP=0.5E-8
      MIN=0.0
      CHECK=1
      INCREASE=1.0
      EOSTART2=1.0
      STEP=5.E-6
      TEST=1
      FACTOR1=STEP/3.0

C return point for new Eostart

5     I=1
      NI=1
```

```
90    K=1
      K2=1.0
      V=0.0
      VSTART=0.0
      FACTOR2=0.0
      IF (EXADD.GT.0.0) GOTO 92
      J=1
92    EO2(I,J)=EOSTART2
      IF (CHECK.LT.0) THEN
              IF (I.EQ.1) THEN
                      XE(1)=TOTAL(1)
                      EX(1)=SQRT(EOSTART2)
                      VX(1)=0.0
                      NI=2
              ELSE
                      XE(NI)=TOTAL(1)
                      EX(NI)=SQRT(EOSTART2)
                      VX(NI)=0.0
                      NI=NI+1
              END IF
      END IF
100   TEMP1=V1*(EXP(V/V1)-EXP(VSTART/V1))
      TEMP1=TEMP1+VSTART-V
      TEMP1=A(I,J)*TEMP1+2.*1.6E-19*V*NT/(12.*8.854E-14)
      TERM=1.0/SQRT(TEMP1+EO2(I,J))
      IF (K.EQ.1) GOTO 130
      IF ((K/2*10).EQ.INT(K2*5)) GOTO 120
      X=FACTOR1*(FACTOR2+TERM)
      E=1.0/TERM
      IF (CHECK.GT.0) GOTO 110
      IF (I.EQ.1) THEN
              X=TOTAL(1)-X
      ELSE
              X=TOTAL(1)+X
      END IF
      XE(NI)=X
      EX(NI)=E
      VX(NI)=V
      NI=NI+1
      IF (I.EQ.1) THEN
              X=TOTAL(1)-X
      ELSE
              X=X-TOTAL(1)
      END IF

110   IF ((X+EXADD).GE.XEND(I,J)) THEN
              J=J+1
              TEMP1=V1*(EXP(V/V1)-EXP(VSTART/V1))
              TEMP1=TEMP1+VSTART-V
              TEMP1=A(I,J)*TEMP1+2.*1.6E-19*NT
              TEMP1=TEMP1*V/(12.*8.854E-14)
              EO2(I,J)=E**2-TEMP1
      END IF
      TERM=2*TERM
      GOTO 130
120   TERM=4*TERM
```

```
130   FACTOR2=FACTOR2+TERM
      V=V+STEP
      IF (V.GE.VEND(I)) GOTO 200
      K=K+1
      K2=K2+1.0
      GOTO 100
200   TOTAL(I)=X
      I=I+1
      IF (I.EQ.2) THEN
              EO2(2,1)=EOSTART2
              STOP=NI-1
              GOTO 90
      END IF
      IF (CHECK.LT.0) GOTO 300
      XT=TOTAL(1)+TOTAL(2)
      DIFF=LENGTH-XT
      IF (DIFF.LT.-1.0E-8) THEN
              IF (TEST2.LT.0) THEN
                      MIN=LENGTH
                      XSTEP=XSTEP/10.0
                      LENGTH=LENGTH+XSTEP
                      EXADD=(TOTLENGTH-LENGTH)/2.0
                      XSTEP=0.5E-8
                      TEST2=1
                      J=1
                      DO M=1,50
                              IF (EXADD.GT.XEND(1,M)) J=M+1
                      END DO
                      GOTO 5
              END IF
      END IF
      IF (DIFF.GT.1.0E-8) THEN
              EOSTART2=EOSTART2-INCREASE
              INCREASE=INCREASE/10.0
              IF (INCREASE.LT.1.0) THEN
                      INCREASE=1.0
                      EOSTART2=1.0
                      IF (FLAT.GT.0) THEN
                              LENGTH=XT
                              EXADD=(TOTLENGTH-LENGTH)/2.0
                              J=1
                              GOTO 5
                      END IF
                      LENGTH=LENGTH-XSTEP
                      IF (LENGTH.LT.MIN) THEN
                              LENGTH=LENGTH+XSTEP
                              XSTEP=XSTEP/10.0
                              LENGTH=LENGTH-XSTEP
                      END IF
                      XSTEP=XSTEP*10.0
                      TEST2=-1
                      EXADD=(TOTLENGTH-LENGTH)/2.0
                      J=1
                      DO M=1,50
                              IF (EXADD.GT.XEND(1,M)) J=M+1
                      END DO
```

```
      GOTO 5
               END IF
               TEST=-1
               GOTO 5
      END IF
      IF (DIFF.LT.-1.0E-8) THEN
               IF (TEST.LT.0) THEN
                        EOSTART2=EOSTART2+INCREASE
                        GOTO 5
               END IF
               INCREASE=INCREASE*10.0
               EOSTART2=EOSTART2+INCREASE
               GOTO 5
      END IF
      IF (CHECK.GT.0) THEN
               CHECK=-1
               GOTO 5
      END IF
300      N=0
      DO J=STOP,1,-1
               N=N+1
               XD(N)=XE(J)
               ET(N)=EX(J)
               VT(N)=VX(J)+(EG/2.0)
      END DO
      DO J=1,N
               XE(J)=XD(J)
               EX(J)=ET(J)
               VX(J)=VT(J)
               VT(J)=VX(J)-EG
      END DO
      DO J=(STOP+1),(NI-1)
               VX(J)=(EG/2.0)-VX(J)
               VT(J)=VX(J)-EG
      END DO
      ADD=0.0
      IF (TOTLENGTH.EQ.LENGTH) GOTO 301
      ADD=TOTLENGTH/2.0-TOTAL(1)
      XSTEP=LENGTH/10000.0
      I=INT(ADD/XSTEP)
      DO J=1,N
               XD(J)=XE(J)
               ET(J)=EX(J)
               VW(J)=VX(J)
               VY(J)=VT(J)
      END DO
      X=XD(N)
      DO J=(N+1),(N+I-1)
               X=X+XSTEP
               XD(J)=X
               ET(J)=0.0
               VW(J)=EG/2.0
               VY(J)=-EG/2.0
      END DO
      XD(J)=TOTLENGTH/2.0
      ET(J)=0.0
```

```
      VW(J)=EG/2.0
      VY(J)=-EG/2.0
      N=N+I+1
      ADD=TOTLENGTH/2.0-TOTAL(2)
      I=INT(ADD/XSTEP)
      X=TOTLENGTH/2.0
      DO J=N,(N+I)
               X=X+XSTEP
               XD(J)=X
               ET(J)=0.0
               VW(J)=EG/2.0
               VY(J)=-EG/2.0
      END DO
      N=N+I+1
      M=STOP+1
      L=NI-1+N-M
      ADD=XD(N-1)-XE(M)
      DO J=N,L
               XD(J)=XE(M)+ADD
               ET(J)=EX(M)
               VW(J)=VX(M)
               VY(J)=VT(M)
               M=M+1
      END DO
      SLOPE=(EG2-EG)/TOTLENGTH
      EXADD=SLOPE
      DO J=1,L
               XE(J)=XD(J)
               EGADD=SLOPE*XE(J)
               GAP(J)=EGADD+EG
               EX(J)=ET(J)+EXADD
               VX(J)=VW(J)
               VT(J)=VY(J)-EGADD
      END DO
      SLOPE=(EG2-EG)/TOTLENGTH
      B=EG
      DO J=1,L
               GO=EXP(G1*(SLOPE*XE(J)+B)+G2)
               LP(J)=2236.07/SQRT(GO)
      END DO
      NI=L+1
301   XSTEP=TOTLENGTH/20.0
      IF (TOTLENGTH.EQ.LENGTH) THEN
               SLOPE=(EG2-EG)/LENGTH
               EXADD=SLOPE
               DO J=1,(NI-1)
                        EGADD=SLOPE*XE(J)
                        GAP(J)=EGADD+EG
                        EX(J)=EX(J)+EXADD
                        VT(J)=VT(J)-EGADD
                        GO=EXP(G1*(SLOPE*XE(J)+B)+G2)
                        LP(J)=2236.07/SQRT(GO)
               END DO
      END IF
      WRITE(6,*) ' EOSTART =',SQRT(EOSTART2)
      WRITE(6,*) ' TOTAL(1) = ', TOTAL(1)
```

```
      XTEST=0.0
      DO I=1,(NI-1)
               IF (XE(I).GE.XTEST) THEN
                WRITE(6,*)XE(I)*1.E4,EX(I),VX(I),VT(I)
                        XTEST=XTEST+XSTEP
               END IF
      END DO
      WRITE(6,*)XE(NI-1)*1E4,EX(NI-1),VX(NI-1),VT(NI-1)
      WRITE(6,*)' '
      XSTEP=LENGTH/1000.0
      XTEST=XSTEP
      STOP=NI-1
      NI=1
      XD(NI)=XE(1)
      ET(NI)=EX(1)
      DO I=2,STOP
               IF (XE(I).GE.XTEST) THEN
315                     NI=NI+1
                        DELY=EX(I)-EX(I-1)
                        DELX=XE(I)-XE(I-1)
                        SLOPE=DELY/DELX
                        B=EX(I)-(SLOPE*XE(I))
                        XD(NI)=XTEST
                        ET(NI)=(SLOPE*XTEST)+B
                        DELY=GAP(I)-GAP(I-1)
                        SLOPE=DELY/DELX
                        B=GAP(I)-(SLOPE*XE(I))
                        GAPC(NI)=(SLOPE*XTEST)+B
                        XTEST=XSTEP*NI
                        IF (XE(I).GE.XTEST) GOTO 315
               END IF
      END DO
      DO I=1,NI
               GO=EXP(G1*(SLOPE*XD(I)+B)+G2)
               LPC(I)=2236.07/SQRT(GO)
      END DO
      TOTPROB(0)=1
      XTEST=0.0
      DO I=1,NI
               EC=0.0258/LPC(I)
               TEMP1=SQRT((ET(I)/EC)**2+4)
               TEMP1=TEMP1/(2.*LPC(I))
               IF (ET(I).LT.0.0) THEN
                        TEMP1=TEMP1+ABS(ET(I)/(2.*LPC(I)*EC))
               ELSE
                        TEMP1=TEMP1-ABS(ET(I)/(2.*LPC(I)*EC))
               END IF
               PROB=EXP(-XSTEP*TEMP1)
               TOTPROB(I)=TOTPROB(I-1)*PROB
               XE(I)=XD(I)
               XTEST=XSTEP*NI
               XPERM(I)=XD(I)
               TOTPROBPERM(I)=TOTPROB(I)
      END DO
      FACTOR1=XSTEP/3.0
      QET=0.0
```

```
      J=0
      B=0.0
      STOP=NI
      DO LAMDA=0.4,0.8,0.02
               SLOPE=(EG2-EG)/TOTLENGTH
               D=EG
               HNU=1.242/LAMDA
               ALPHA1=0.0
               FIRST=-1
               SECOND=-1
               THIRD=-1
               QEW=0.0
               N=1
               X=1.0
410            FACTOR2=0.0
               K=0
               K2=0.0
               J=J+1
               B=B+1.0
               DO I=1,STOP
               IF (XE(I).LT.0.0) XE(I)=0.0
               K=K+1
               K2=K2+1.0
               GAP(I)=SLOPE*XD(I)+D
               IF ((HNU-GAP(I)).GT.0.1) THEN
                ALPHA2=((750*(HNU-GAP(I)))**2)/HNU
                IF (ALPHA2.GT.4.E5) THEN
                                    DALPHAX=4.E5
                                    ALPHAX=4.E5*XE(I)
                                    GOTO 415
                END IF
                TEMP1=750**2/HNU
                TEMP2=(HNU-GAP(I))**2
                ALPHAX=ALPHA2*XE(I)
                TEMP1=TEMP1*TEMP2
                TEMP2=2.*TEMP1*XE(I)*(-SLOPE)
                DALPHAX=TEMP1+TEMP2
               ELSE
                C1=(750**2)*0.01
                TEMP1=-C1/(GAP(I)+0.1)**2
                TEMP1=TEMP1*EXP(-(GAP(I)+0.1)/0.045)*SLOPE
                TEMP2=-C1*SLOPE/0.045
                TEMP2=TEMP2/(GAP(I)+0.1)
                TEMP2=TEMP2*EXP(-(GAP(I)+0.1)/0.045)
                C3=C1/(GAP(I)+0.1)
                C3=C3*EXP(-(GAP(I)+0.1)/0.045)
                DALPHAX=(TEMP1+TEMP2)*EXP(HNU/0.045)*XE(I)
                DALPHAX=DALPHAX+C3*EXP(HNU/0.045)
                ALPHAX=C3*EXP(HNU/0.045)*XE(I)
               END IF
415                     TEMP2=DALPHAX*EXP(-ALPHAX)
                        TERM=TOTPROB(I)*TEMP2
                        IF (I.EQ.1) GOTO 430
                        IF (I.EQ.STOP) GOTO 430
                        IF ((K/2*10).EQ.INT(K2*5.)) GOTO 420
                        TERM=2*TERM
```

```
                GOTO 430
420                     TERM=4*TERM
430                     FACTOR2=FACTOR2+TERM
                END DO
                QE=FACTOR1*FACTOR2
                IF (N.EQ.1) GOTO 440
                QE=QE*(0.9**(N-1))*(0.8**(N-2))
440             QEW=QEW+QE
                M=0
                IF (QE.LT.1.E-5) THEN
                        IF ((N/2*10).NE.INT(X*5.)) GOTO 500
                END IF
                X=X+1.0
                N=N+1
                IF ((N/2*10).EQ.INT(X*5.)) THEN
                        D=EG2
                ELSE
                        D=EG
                END IF
                SLOPE=-SLOPE
                DO I=STOP,1,-1
                        M=M+1
                        VT(M)=XE(M)+TOTLENGTH
                        TOTPROBC(M)=TOTPROB(I)
                        XB(M)=XD(I)
                END DO
                DO I=1,STOP
                        XD(I)=TOTLENGTH-XB(I)
                        XE(I)=VT(I)
                        TOTPROB(I)=TOTPROBC(I)
                END DO
                GOTO 410
500             WRITE(6,*)' QE = ',QEW,' LAMDA = ',LAMDA,X
                DO I=1,STOP
                        XE(I)=XPERM(I)
                        XD(I)=XPERM(I)
                        TOTPROB(I)=TOTPROBPERM(I)
                END DO
                IF (J.EQ.1) GOTO 530
                IF (J.EQ.21) GOTO 530
                IF ((J/2*10).EQ.INT(B*5.0)) GOTO 520
                QEW=2*QEW
                GOTO 530
520             QEW=4*QEW
530             QET=QET+QEW
        END DO
        QET=QET*(.02/3.0)/0.4
        WRITE(6,*)' QET = ',QET
600     CONTINUE
        END
```